July 17, 2006

Summertime influence of Asian pollution in the free troposphere over North America

Q. Liang[1], L. Jaeglé[1], R. C. Hudman[2], S. Turquety[2], D. J. Jacob[2], M. Avery[3], D. R. Blake[4], E.V. Browell[3], G. Sachse[3], W. Brune[5], X. Ren[5], A. Clarke[6], R. Cohen[7], J. Dibb[8], A. Fried[9], H. Fuelberg[10], M. Porter[10], B. Heikes[11], G. Huey[12], H. Singh[13], P. Wennberg[14]

[1] Department of Atmospheric Sciences, University of Washington, Box 351640, Seattle, WA 98195-1640, USA.
[2] Division of Engineering and Applied Science, Harvard University, Pierce Hall, 29 Oxford Street, Cambridge, MA 02138, USA.
[3] NASA Langley Research Center, Hampton, VA 23681, USA.
[4] Department of Chemistry, University of California, Irvine, CA 92697, USA.
[5] Department of Meteorology, Pennsylvania State University, 503 Walker Building, University Park, PA 16802, USA.
[6] Department of Oceanography, University of Hawaii at Manoa, Honolulu, HI 96822, USA.
[7] Department of Chemistry, University of California, Berkeley, CA 94720, USA.
[8] University of New Hampshire, Climate Change Research Center, 39 College Road, Durham, NH 03824, USA.
[9] Atmospheric Chemistry Division, National Center for Atmospheric Research, Boulder, Colorado 80307-3000, USA.
[10] Department of Meteorology, Florida State University, Tallahassee, FL 32306-4520, USA.
[11] Department of Oceanography, University of Rhode Island, Narragansett, Rhode Island 02881, USA.
[12] School of Earth and Atmospheric Sciences, Georgia Institute of Technology, Atlanta, GA 30332-0340, USA
[13] NASA Ames Research Center, MS-245-5, Moffett Field, CA 94035, USA.
[14] California Institute of Technology, MC 150-21, 1200 E. California Blvd, Pasadena, CA 91125, USA.

Abstract

We analyze aircraft observations obtained during INTEX-A (1 July – 14 August 2004) to examine the summertime influence of Asian pollution in the free troposphere over North America. By applying correlation analysis and Principal Component Analysis (PCA) to the observations between 6-12 km, we find dominant influences from recent convection and lightning (13% of observations), Asia (7%), the lower stratosphere (7%), and boreal forest fires (2%), with the remaining 71% assigned to background. Asian airmasses are marked by high levels of CO, O_3, HCN, PAN, acetylene, benzene, methanol, and SO_4^{2-}. The partitioning of reactive nitrogen species in the Asian plumes is dominated by PAN (~600 pptv), with varying NO_x/HNO_3 ratios in individual plumes consistent with different plumes ages ranging from 3 to 9 days. Export of Asian pollution in warm conveyor belts of mid-latitude cyclones, deep convection, and lifting in typhoons all contributed to the five major Asian pollution plumes. Compared to past measurement campaigns of Asian outflow during spring, INTEX-A observations display unique characteristics: lower levels of anthropogenic pollutants (CO, propane, ethane, benzene) due to their shorter summer lifetimes; higher levels of biogenic tracers (methanol and acetone) because of a more active biosphere; as well as higher levels of PAN, NO_x, HNO_3, and O_3 (more active photochemistry possibly enhanced by injection of lightning NO_x). The high $\Delta O_3/\Delta CO$ ratio (0.76 mol mol^{-1}) of Asian plumes during INTEX-A is due to a combination of strong photochemical production and mixing with stratospheric air along isentropic surfaces. The GEOS-Chem global chemical transport model captures the timing and location of the Asian plumes remarkably well. However, it significantly underestimates the magnitude of the enhancements.

1. Introduction

Many field campaigns and modeling studies have shown significant influences of transpacific transport of Asian pollution over North America during spring [e.g. *Andreae et al.*, 1988; *Kritz et al.*, 1990; *Parrish et al.*, 1992, 2004; *Berntsen et al.*, 1999; *Yienger et al.,* 2000; *Jacob et al*., 1999; *Jaffe et al.*, 1999, 2003; *Nowak et al*., 2004]. Not much attention has been paid to summertime transpacific transport, which is expected to be inefficient due to slow large-scale flow and short lifetimes of many trace gases. However, modeling studies have shown that even a small influence of Asian emissions over North America during summer can have significant implications for air quality regulation. *Fiore et al.* [2002] found that anthropogenic emissions from Asia and Europe contribute 4-7 ppbv to summertime afternoon O_3 concentrations in surface air over the U.S., potentially causing violations of the air quality standard. *Jacob et al.* [1999] showed that tripling of Asian anthropogenic emissions from 1985 to 2010 will increase surface O_3 in the United States (U.S.) by 1-5 ppbv during summer.

Long-range transport of Asian pollution across the Pacific reaches a maximum in spring due to active cyclonic activity and strong westerly winds. The strongest Asian outflow occurs in the middle troposphere [*Bey et al.*, 2001b; *Stohl*, 2001; *Stohl et al.*, 2002; *Liu et al.*, 2003] and can be transported across the Pacific in 5-10 days [*Jaffe et al.*, 1999, 2001; *Yienger et al.*, 2000; *Stohl et al.*, 2002; *Liang et al.*, 2004]. During summer, export of Asian pollution by convection competes with export in mid-latitude cyclones, and transpacific transport occurs predominantly in the middle and upper troposphere with an average transpacific transport time of 6-10 days [*Liang et al.*, 2004; *Holzer et al.*, 2005]. In addition, a significant fraction of the summertime Asian outflow is transported westward to the Middle East rather than to the Pacific [*Liu et al*.,

2002, 2003; *Lelieveld et al.*, 2002]. The weaker Aleutian low during summer also leads to relatively slow and weak transport across the Pacific [*Liang et al.,* 2005; *Holzer et al.*, 2005].

The Intercontinental Chemical Transport Experiment-Phase A (INTEX-A) aircraft mission was conducted during the summer of 2004 and focused on quantifying and characterizing the summertime inflow and outflow of pollution over North America [*Singh et al.*, this issue]. INTEX-A was part of the larger International Consortium for Atmospheric Research on Transport and Transformation (ICARTT) multi-platform field campaign aimed at examining regional air quality, intercontinental transport, and radiation balance in the atmosphere.

During the INTEX-A mission several Asian plumes were predicted by forecast chemical transport models (CTMs) and then sampled by aircraft, displaying enhanced levels of many trace gases and aerosols. INTEX-A observations thus offer the unprecedented opportunity to quantify the role of transpacific transport of Asian pollution during summer. In this study we will analyze these observations to examine the chemical composition transport mechanisms of these plumes and contrast them to springtime observations. Section 2 describes the observations and the model used in this study. In section 3 we use Principal Component Analysis (PCA) to identify characteristic airmasses, in particular airmasses influenced by Asian pollution. Transport mechanisms and chemical characteristics of the Asian plumes observed during INTEX-A are discussed in detail in section 4. Conclusions are presented in Section 5.

2. Observations and Model

2.1 Observations

A total of 18 flights were made by NASA's DC-8 aircraft between 1 July and 14 August 2004 during INTEX-A. The flights took place mostly over the United States, extending to the

Pacific Ocean in the west and Atlantic Ocean to the east. Flight tracks are shown on Figure 3. In situ observations included an extensive suite of measurements of ozone, aerosols and their precursors, as well as long-lived greenhouse gases, and many meteorological and optical parameters. Table 1 summarizes the in situ observations used in this paper. We also use remote sensing of ozone and aerosols (both zenith and nadir) on board the DC-8 with the Differential Absorption Lidar (DIAL) [*Browell et al.*, 2003].

Some measurements were measured by two different techniques (HNO_3 and H_2O_2), when both are available we average them. On several occasions, CO measurements were not available. CO is critical as a tracer of long-range transport in our analysis. As CO and C_2H_2 are highly correlated (r = 0.92 for all INTEX-A measurements), we replace these missing CO values with values derived based on observed C_2H_2-CO relationship: CO (ppbv) = 73 + 0.3336 * C_2H_2 (pptv).

In order to examine the transport of Asian plumes across the Pacific, we complement these aircraft observations with space-based observations of CO from the Measurements of Pollution In The Troposphere (MOPITT) instrument [*Drummond and Mand*, 1996] on board Terra. We use the level 2 V3 datasets that consist of retrieved CO mixing ratios at 7 vertical levels in the atmosphere (surface to 150 hPa). However, the global average number of degrees of freedom in the MOPITT vertical profiles is less than 2 with strongest sensitivity in the middle troposphere [*Deeter et al.*, 2003, 2004].

2.2 Model description

GEOS-Chem CTM is driven by assimilated meteorological data compiled at the Goddard Earth Observing System (GEOS) of the NASA Global Modeling and Assimilation Office. The GEOS-4 meteorological fields have a horizontal resolution of 1°x1.25° and 55 vertical layers. We regrid the data into a horizontal resolution of 2°x2.5° and merge the upper 26 sigma layers

(<30 hPa) into one layer for computational efficiency. The surface and upper level meteorological fields are updated every 3 and 6 hours, respectively. For this study, we use model version v7.02.04 (http://www-as.harvard.edu/chemistry/trop/geos/index.html).

The GEOS-Chem model simulates ozone-NO_x-hydrocarbon-aerosol chemistry and involves 50 tracers, over 80 chemical species and 300 reactions. The ozone simulation [*Bey et al.,* 2001a; *Martin et al.*, 2002] is fully coupled to the aerosol simulation that includes sulfate-nitrate-ammonium, organic and black carbon, soil dust, and sea salt [*Park et al.,* 2003, 2004; *Alexander et al.*, 2005; *Fairlie et al.*, 2006]. We use a base anthropogenic emission inventory for 1985 based on Global Emission Inventory Activity (GEIA) and scaled to 1998 following *Bey et al.* [2001a]. We use the updated U.S. Environmental Protection Agency (EPA) 1999 National Emission Inventory (NEI-99, http://www.epa.gov/ttn/chief/net/1999inventory.html) over the U.S. with a 50% decrease based on the ICARTT observations [*Hudman et al.*, this issue]. Large fires occurred over Alaska and Canada during INTEX-A [*Pfister et al.*, 2005; *Morris et al.*, this issue]. We use daily biomass burning emissions over North America derived using Moderate Resolution Imagine Spectroradiometer (MODIS) Active Fire and the area burned as reported by the National Interagency Coordination Center (NICC), contributing 27 Tg CO between 1 June and 31 August 2004, 3 times the climatology (9 Tg CO) [*Turquety et al.*, this issue]. Elsewhere, we use the monthly varying climatological biomass burning inventory of *Duncan et al.* [2003]. Biofuel emissions are described by *Yevich and Logan* [2003]. Soil NO_x emissions are based on *Yienger and Levy* [1995] as described in *Wang et al.* [1998]. We include a lightning NO_x source of 7.1 TgN/yr [*Hudman et al.* this issue; *Martin et al.,* this issue]. A more detailed description of the model as applied to ICARTT observations is given in *Hudman et al.* [this issue] and *Turquety et al.* [this issue].

In addition to the standard full chemistry simulation, we conduct a tagged CO simulation [*Bey et al.*, 2001b; *Liu et al.* 2003; *Li et al.*, 2005] using archived monthly OH fields from the full chemistry simulation. We transport a suite of six CO tracers to track emissions from individual source regions and types: Asian anthropogenic, Asian biomass burning, North American anthropogenic (combining both fossil fuel and biofuel emissions), North American biomass burning, European anthropogenic, and the rest of the world. We use "Asian CO" to refer to CO emitted over East Asia (defined as the 66° - 146°E, 9°S - 90°N region), including both anthropogenic and biomass burning emissions. The contribution of climatological Asian biomass burning emissions is small, accounting for 26% of Asian CO during summer.

GEOS-Chem has been validated by numerous comparisons to observations, showing no model biases [*Li et al.*, 2002, 2004; *Heald et al.*, 2003; *Fiore et al.*, 2002; *Park et al.*, 2003; *Duncan and Bey*, 2004]. Of particular interest to our study, the model has been used to examine outflow of Asian pollution to the Pacific [*Bey et al.*, 2001b; *Liu et al.*, 2002, 2003; *Palmer et al*., 2003] and trans-Pacific transport to North America [*Heald et al.*, 2003, 2006; *Jaeglé et al.*, 2003; *Liang et al.*, 2004, 2005; *Weiss-Penzias et al.*, 2004; *Jaffe et al.*, 2004; *Hudman et al.*, 2004; *Bertschi et al.*, 2004; *Park et al.*, 2004].

Several studies use the GEOS-Chem model to interpret ICARTT observations. *Hudman et al.* [this issue] examine the North American nitrogen budget. *Turquety et al.* [this issue] constrain boreal forest fire emissions by combining the model together with MOPITT observations. *Martin et al.* [this issue] use the model to evaluate a new space-based NO_x emissions inventory by comparison to ICARTT observations. *Millet et al.* [this issue] combine in situ and satellite measurements of HCHO to constrain the isoprene emissions in the model.

3. Airmass identification

3.1 Biomass burning influence

Several biomass burning plumes from Canadian and Alaskan fires were sampled during INTEX-A in the lower and middle troposphere. We identify observations with CO > 170 ppbv or HCN > 560 pptv as biomass burning plumes. We confirmed the validity of this method by examining results from the tagged CO simulation as well as back trajectories. We find that 2% of the INTEX-A observations in the middle and upper troposphere (6-12 km) were influenced by emissions from boreal forest fires. The biomass burning airmasses display large enhancements in many trace gases: CO, hydrocarbons (ethene, benzene, C_2H_2, methanol, toluene, ethanol, acetaldehyde, ethane), reactive nitrogen species (PAN, PNs), HCN, CH_3CN, as well as smaller enhancements in CH_3OOH, H_2O_2, and CH_4 (Table 2). These airmasses also display elevated concentrations of aerosols ionic species: sulfate (SO_4^{2-}), nitrate (NO_3^-), ammonium (NH_4^+), as well as oxalate ($C_2O_4^{2-}$) and potassium (K^+). Such enhancements in biomass burning plumes have been commonly observed in previous studies [e.g. *Goode et al.,* 2000; *Cofer et al.*, 1998; *Singh et al,* 2004; *Bertschi et al.*, 2004; *Dibb et al*., 2003b].

3.2 Principal component analysis

For the remaining observations, we apply Principal Component Analysis (PCA) to objectively identify the origin of airmasses. PCA is a mathematical technique that reduces the dimensions of a dataset based on covariance of variables, and has been applied to source identification in numerous air quality studies [*e.g. Thurston and Spengler,* 1985; *Buhr et al.*, 1995; *Statheropoulos et al.*, 1998; *Guo et al*., 2004]. A typical approach is to extract preliminary factors using PCA and then obtain the final physically realizable structures through rotations of the preliminary factors. For this work, we use the rotated principal component analysis (RPCA)

by *Lin and Arakawa* [2000], which uses Promax rotation with a revised manipulation to reduce the deficiency introduced by the linear Promax model and to improve the capability in recovering embedded structures of data.

We first construct our data matrix by using 9 observed chemical variables from a 1-min merged data set of observations obtained between 6 and 12 km altitude: O_3, CFC-11, CFC-12, NO_x ($NO+NO_2$), the NO_x/HNO_3 ratio, H_2O_2, CO, HCN, and PAN. Through a systematic correlation analysis for all observed species, we found that these 9 variables display the highest intercorrelations indicating they are good tracers for identification of airmass origin. These variables are also chosen because they contain the least number of missing values. We apply our analysis to 3633 1-min observations, 87% of the observations obtained between 6-12 km during INTEX-A.

The PCA yields three leading Empirical Orthogonal Functions (EOF) representing distinct patterns. The relative contribution of each EOF to an individual 1-min measurement point is contained in the corresponding principal component (PC) value. We define a measurement point as being dominated by a specific EOF when its PC is greater than one standard deviation (1σ) and other PCs are $< 1\sigma$. The EOF patterns are shown in Figure 1, while the chemical composition of each corresponding type of airmass is listed in Table 2. Chemical species that are significantly enhanced ($>$ mean$+1\sigma$) or depleted ($<$ mean-1σ) compared to background levels are highlighted in bold in Table 2.

Based on these EOFs, we segregated air sampled between 6-12 km during INTEX-A into 4 major categories: (1) lower stratospheric air (7% of observations), (2) convection/lightning (13%), (3) Asian (7%), and (4) biomass burning (2%, from the correlation analysis, see section

3.1). Airmasses not included in any of the above categories were classified as "background" air (71%) (Table 2).

The first EOF represents air with enhanced O_3 concentrations and is depleted in CFC-11 and CFC-12, consistent with a lower stratospheric influence (Figure 1). We find that the stratospheric airmasses contain enhanced levels of HNO_3 (677±340 pptv versus 245±210 pptv in background air), SO_4^{2-} (100±36 pptv versus 60±42 pptv), ^7Be (2994±1754 fCi/m^3 versus 497±675 fCi/m^3), and low relative humidity (RH) (23.7±19.9 % versus 48.5±26.8 %), CH_4 (1757±34 ppbv versus 1791±16 ppbv), CFC-113 (75.8±1.7 pptv versus 78.4±0.6 pptv), H-1211 (4.06±0.21 pptv versus 4.32±0.11 pptv) (Table 2).

The second EOF contains enhanced NO_x concentrations and NO_x/HNO_3 ratios, which are correlated with low concentrations of H_2O_2 (Figure 1), indicating fresh convection (HNO_3 and H_2O_2 are scavenged because of their high solubility) accompanied by lightning (elevated NO_x). This airmass type is characterized by elevated anthropogenic tracers, in particular SO_2 (51±79 pptv versus 33±45 pptv), ethane (977±510 pptv versus 715±268 pptv), propane (280±269 pptv versus 138±124 pptv), toluene (8±3 pptv versus 5±2 pptv), and C_2H_2 (95±36 pptv versus 80±31 pptv) (Table 2). It also contains high levels of methanol and ethanol, which have biogenic land sources [*Singh et al.*, 2000; *Heikes et al.*, 2002]. It displays a higher NO_x/HNO_3 ratio (1.26±0.93 v/v) compared to background air (0.38±0.32 v/v) as a result of recent ventilation of NO_x from boundary layer by deep convection, as well as NO_x formation in lightning.

The third EOF is significantly enhanced in CO, HCN, and PAN without any NO_x enhancements (Figure 1). This EOF is consistent with aged transport plumes from East Asia, as we will see below by examining their chemical composition. The Asian origin for these plumes

is confirmed by independent analyses with the GEOS-Chem tagged simulation and back trajectories (section 4.1).

The Asian airmasses are significantly enhanced in many trace gases associated with fossil fuel combustion, in particular CO (128±14 ppbv, 35% increase with respect to background), C_2H_2 (159±40 pptv, 99%), HCN (420±60 pptv, 47%), and benzene (24±11 pptv, 85%) (Table 2). Species with biogenic sources are also found to be enhanced in the Asian plumes: methanol (2.2±1.0 ppbv, 67%) and acetone (2±1 ppbv, 39%). Enhanced mixing ratios of O_3 (99±20 ppbv, 36%) and PAN (592±159 pptv, 97%) in the Asian plumes, indicate efficient photochemistry. The Asian airmasses also display enhanced levels of aerosol species associated with anthropogenic emissions: SO_4^{2-} (111±55 pptv, 85%) and NH_4^+ (130±61 pptv, 86%). In addition, levels of oxalate, $C_2O_4^{2-}$ (15±7 pptv, 150%), which has been linked to biomass or biofuel burning [*Dibb et al.*, 2003b] are also elevated.

Al-Saadi et al. [this issue] presented a Lagrangian analysis of air influencing the U.S. during INTEX-A using 10-day back trajectories and found that of 9% of the entire U.S. domain between 6-12 km during ICARTT was influenced by East Asian air, 12% by stratospheric air, and 13% by strong convection, consistent with our results.

3.3 Trace gas relationships

Figure 2 shows trace gas relationships for these 5 airmasses. The airmasses with lower stratospheric influences show strong negative CO-O_3 (r = -0.80, 99% significant) and CO-HNO_3 (r = -0.69, 99%) relationships, and a weaker positive O_3-NO_y relationship (r = 0.41, 99%). The Convection/Lightning category displays positive correlation between anthropogenic pollutants, i.e. CO, C_2H_2, and PAN, a negative CO-HNO_3 correlation (-0.44, 99%) and no significant correlation between CO and O_3 (r = 0.18), indicating freshly ventilated pollution with scavenging

of HNO_3 and little O_3 production. Biomass burning plumes contain highly correlated CO, PAN, HCN, C_2H_2, SO_4^{2-} (r = 0.72 – 0.99, 99%) with weak negative CO-O_3 and CO-HNO_3 correlations (r = -0.44 and -0.42, respectively, 99%).

The Asian airmasses show strong positive CO-PAN (r = 0.69, 99%) and CO-C_2H_2 (r = 0.78, 99%) correlations, as commonly observed in anthropogenic transport plumes [e.g. *Singh et al.,* 1995]. While CO and HCN are significantly enhanced in the Asian airmasses (Table 2), these tracers are only weakly correlated (r = 0.41, 99%) with a slope of 0.87e-3 mol mol^{-1}, half the value observed in the Chinese urban plumes during TRACE-P (1.67e-3 mol mol^{-1}) [*Li et al.*, 2003]. This weak correlation and small HCN-CO enhancement ratio suggest mixing of domestic coal burning together with non-coal fossil fuel emissions [e.g. *Singh et al.,* 2003; *de Gouw et al.*, 2003].

We find that CO and NO_y are moderately correlated (r=0.30, $\Delta NO_y/\Delta CO$=8±2 pptv/ppbv). CO and O_3 are positively correlated (r = 0.53) with a $\Delta O_3/\Delta CO$ ratio of 0.76 ± 0.04 mol mol^{-1}. O_3 and NO_y are also positively correlated (r = 0.51, $\Delta O_3/\Delta NO_y$ =0.1±0.01 mol mol^{-1}). These positive correlations are indicative of efficient NO_y export from Asia followed by active photochemical ozone production (section 4.3). The Asian airmasses do not display consistent relationships between CO and HNO_3, and CO and SO_4^{2-} ($r_{CO,HNO3}$ = 0.36, $r_{CO,SO4=}$ = -0.09), likely reflecting different chemical and wet scavenging histories for individual plumes.

4. Asian Plumes

We identify 5 major Asian plumes during INTEX-A: 1 July, 15 July, 20 July, 2 August, and 14 August 2004. Figure 3 (panel a) shows the location of these plumes, color coded by observed

CO levels. The plumes extend from the Northeastern (NE) Pacific to Northwestern (NW) Atlantic.

4.1 Identification with other methods

We verify the PCA Asian airmass identification by using the GEOS-Chem tagged Asian CO tracer sampled along the flight tracks. Because of the dispersion of Asian plumes as they cross the American continent [*Li et al*., 2006], we use a longitude-dependent threshold for Asian CO linearly decreasing from 30 ppbv at 125°W to 16 ppbv at 65°W. We identify the same 5 Asian plumes and we find that 9% (330 minutes) of observations were influenced by Asian emissions (compared to 7% from PCA). The broad picture of geographic distribution of the Asian plumes agrees well between PCA and GEOS-Chem (Figure 3, panels a and b). There are differences in the detailed location of the plumes, likely from transport errors resulting from coarse model resolution and numerical diffusion in the model. If we allow an overlap time window of ±10 minutes along the flight tracks (~ 70 km horizontal displacement) to account for transport error, we find that 85% of the Asian plumes identified by PCA overlap with those identified by GEOS-Chem. The overlap increases to 95% when the time window is increased to ±30 minutes.

We further verify our PCA results with 10-day kinematic back trajectories calculated with the Florida State University (FSU) kinematic model [*Fuelberg et al.*, 2003] using reanalysis data from the National Weather Service's Global Forecast System (GFS). The reanalysis data were available 4 times daily, with 26 vertical levels and a horizontal resolution of T254, which was interpolated to a 0.5°x0.5° horizontal grid [*Fuelberg et al*., this issue]. The trajectories were calculated for each minute along the flight tracks. Measurements with back trajectories that overpass the heavily polluted region in East Asia (90-140°E, 20-55°N) within 10 days are identified as Asian plumes. This method yields a very similar geographical distribution of Asian

plumes (Figure 3, panel c) compared to the PCA and GEOS-Chem methods. It identifies 11% (403 minutes) of the observations as Asian plumes. We find that 95% of the Asian plumes identified by the PCA overlap with those identified using back trajectories within ±10 minutes, and the overlap increases to 99% within ±20 minutes.

Both GEOS-Chem and back trajectories identify more observations with Asian influence (9% and 11% of observations, respectively) compared to the observation-based PCA (7%). With the coarse vertical resolution (~1 km) of the meteorological fields used in these analyses it is not possible to accurately represent the thin layers (~few hundred meters) of pollution plumes crossing the Pacific [e.g. *Brock et al.*, 2004; *de Gouw et al.*, 2004]. Instead both the model and back trajectories are spreading the Asian plumes over thicker layers, and thus overestimate their vertical extent and their overall influence.

4.2 Transport mechanisms

Fuelberg et al. [this issue] compared the mean meteorological conditions during INTEX-A to the mean climatology for the 2000 – 2004 summers and found a stronger than normal Alaskan ridge. This configuration favors long-range transport across the Pacific [*Liang et al.*, 2005]. The 300 hPa winds during 2004 were not significantly different from climatology.

We identify the transport mechanisms of the Asian plumes in two steps. We first determine transport time by tracking Asian plumes from the sampling location back to Asia using the GEOS-Chem tagged CO simulation. The transport time is verified using the FSU back-trajectories. In a second step we examine export mechanisms using the GEOS-4 convective diagnostics, sea level pressure fields and detailed synoptic charts with frontal and typhoon positions from the NCEP weather maps at the National Climatic Data Center (http://www.ncdc.noaa.gov/oa/ncdc.html).

The transport characteristics of the 5 major Asian plumes observed during INTEX-A are summarized in Table 4. The plumes have varying transit times across the Pacific (3-9 days) and transport altitudes (6 to 11.5 km). The shortest transport times correspond to the two strongest plumes observed during INTEX-A: 3-5 days from Asia to the NE Pacific for the 1 July event and 5-9 days from Asia to the U.S. East Coast for the 2 August event.

The export mechanisms of these Asian plumes are lifting in warm conveyor belts (WCB) of mid-latitude cyclones (1 July, 15 July, 20 July, and 14 August) and deep convection (1 July and 2 August). During August, which marks the beginning of the typhoon season for East Asia, we find that lifting in typhoons also plays an important role in the export two Asian plumes (2 and 14 August). The role of typhoons in inducing rapid lofting of surface pollution in the upper troposphere was observed during PEM-West A [*Newell et al.*, 1996; *Blake et al.*, 1996] and discussed by *Liang et al.* [2004].

4.3 Chemical composition: Comparison to previous campaigns

Table 3 compares the chemical composition of the Asian airmasses sampled during INTEX-A with four springtime measurement campaigns: PEM–West B (February – March 1994) [*Hoell et al.*, 1997], TRACE-P (February – April 2001) [*Jacob et al.*, 2003], ITCT 2K2 (April – May 2002) [*Parrish et al.*, 2004], and PHOBEA (Springs 1997-2002) [*Jaffe et al.*, 2001]. The summertime Asian plumes observed during INTEX-A display a distinct chemical signature compared to these springtime measurements. They contain systematically lower levels of anthropogenic tracers (CO, ethane, propane, C_2H_2, and benzene: 128±14 pptv, 882±193 pptv, 159±40 pptv, 24±11 pptv) compared to springtime Asian outflow (134-198 pptv, 1243-1600 pptv, 264-319 pptv, 54-100 pptv) consistent with a shorter lifetime of these tracers during summer. Methanol and acetone levels (2.2±1.0 ppbv and 2±1 ppbv, respectively) are higher than during

spring (0.72-1.8 ppbv and 0.57-1.4 ppbv, respectively). Both tracers have strong biogenic source during summer [*Singh et al*., 1994; 2000; *Heikes et al*., 2002]. In their global simulation, *Jacob et al*. [2005] found a late spring-summer maximum in methanol surface concentrations (> 5-10 ppbv) over mid-latitudes. Surface concentrations were particularly elevated North of 35°N over Asia in July due to the late emergence of leaves and the long continental fetch. INTEX-A observations of elevated methanol in Asian plumes are thus consistent with mixing of large biogenic emissions in the anthropogenic outflow.

The INTEX-A Asian plumes contain levels of reactive nitrogen species significantly higher than previously observed (Table 3): PAN (592±159 pptv compared to 210-360 pptv for springtime campaigns), HNO_3 (363±304 pptv compared to 70-234 pptv), and NO_x (289±201 pptv compared to 48-90 pptv). Overall, the mixing ratios of NO_y (1330±458 pptv) are a factor of 2 larger than observed during these previous campaigns (528-640 pptv). We examine below four possible causes for these high NO_y levels during summer relative to spring: more efficient NO_y export efficiency, higher surface NO_x emissions, recent mixing with NO_x from local convection/lightning over the U.S., influence of lightning over East Asia.

In their modeling study over N. America, *Liang et al.* [1998] found little seasonality in the NO_y export efficiency from the polluted boundary layer, with similar export efficiencies during summer and spring (25%). If we can extrapolate these results to East Asia, it seems that variability in NO_y export efficiency is unlikely. Based on satellite observations, Chinese emissions appear to have a wintertime maximum and summer minimum [*Jaeglé et al.*, 2005; *Richter et al.*, 2005; *Martin et al.*, this issue]. The higher NO_x mixing ratios during INTEX-A could be due in part to mixing with high background NO_x over North America influenced by local lightning [*Hudman et al.*, this issue; *Martin et al*., this issue; *Cohen et al.*, this issue]. Table

2 shows that NO_x levels in the Asian plumes (289 pptv) are similar to background air (285 pptv). However, when we restrict our analysis to plumes sampled over the NE Pacific on July 1 during INTEX-A, we still find relatively high levels of NO_x (145 pptv, Table 4, see section 4.4). In addition, the low NO_x/HNO_3 in Asian airmasses (0.3 mol/mol) indicates aged plumes compared to those influenced by local convection/lightning (1.26 mol/mol). Lightning is expected to be more frequent during summer. The generally strong correlation in the Asian plumes between CO and PAN (r=0.69) but a much weaker correlation between CO and NO_y (r=0.30) suggest that export of anthropogenic NO_y, mostly in the form of PAN [*Bey et al.*, 2001b; *Li et al*., 2006], has been mixed with fresh NO_x emissions from lightning either over Asia or over the western Pacific.

Despite the difference in total reactive nitrogen, we find a similar partitioning among NO_y species, with PAN being the dominant reactive nitrogen species, accounting for 44% of NO_y during INTEX-A, compared to 40% for PEM-West B, 45% for TRACE-P, and 56% for ITCT2K2.

Aerosol ionic concentrations of SO_4^{2-}, NO_3^-, and NH_4^+ in the Asian plumes observed during INTEX-A are similar as those observed during TRACE-P and ITCT2K2. Springtime measurements obtained during TRACE-P and ITCT2K2 display higher levels of Ca^{2+} (118 pptv and 73 pptv, respectively) than those observed during summer 2004 (31 pptv). Elevated Ca^{2+} concentrations are characteristic of dust emissions [*Dibb et al.*, 2003b; *Kline et al.*, 2004], which maximize in spring over East Asia [e.g. *Merrill et al.*, 1989; *Husar et al.*, 2001]. ITCT2K2 observations show high levels of K^+ (75 pptv, compared to 21 pptv during INTEX-A) as well as CH_3CN (310 pptv, compared to 158 pptv during INTEX-A), due to long-range transport of biomass burning emissions from SE Asia, which also maximize in spring [*Nowak et al.*, 2004; *de Gouw et al.*, 2004; *Brock et al.*, 2004].

The observed $\Delta O_3/\Delta CO$ ratio in the Asian plumes during INTEX-A (0.76 ± 0.04 mol mol^{-1}) is higher than the values observed in Asian plumes over the NE Pacific during spring: $\Delta O_3/\Delta CO$=0.37 mol mol^{-1} for PHOBEA [*Price et al.,* 2004] and $\Delta O_3/\Delta CO$=0.10 mol mol^{-1} for ITCT2K2 [*Nowak et al.,* 2004]. Ozone production in the upper troposphere over East Asia reaches its maximum during summer because of rapid vertical transport of ozone precursors [*Liu et al*., 2002]. Similar $\Delta O_3/\Delta CO$ enhancements ratios (>0.7 mol mol^{-1}) were reported in the upper troposphere downwind of Asia for July using CO and O_3 from the Tropospheric Emission Spectrometer (TES) instrument [Zhang et al., 2006]. *Mauzerall et al.* [2000] found a near doubling in net ozone production over East Asia during summer compared to spring.

In addition, some Asian plumes observed during INTEX-A exhibit mixing with stratospheric air (see section 4.4), further enhancing O_3 levels. During summer at mid-latitudes, stratosphere-troposphere exchange occurs mostly along isentropic surfaces that intersect the tropopause [*Scott and Cammmas*, 2002; *Jing et al.,* 2004]. The transport of Asian pollution in the upper troposphere over the Pacific is thus subject to mixing with lower stratospheric air.

4.4 Variability in individual plumes and case studies

Individual Asian plumes all have in common enhancements in CO, PAN, HCN, C_2H_2, and methanol but they display varying levels of O_3, HNO_3, and H_2O_2, as well as aerosol concentrations of SO_4^{2-}, NO_3^-, and NH_4^+ (Table 4). Below we contrast the two strongest Asian plumes observed on the 1 July and 2 August 2004 flights.

The 1 July 2004 Asian long-range transport event is remarkable because of its very short transport time of 3-5 days, which is faster than many trans-pacific transport events during spring [*Jaffe et al.*, 2003]. Both the GEOS-Chem Asian CO tracer (Figure 4) and the kinematic back trajectories (Figure 5) indicate that this episode is the result of two separate transport plumes:

plume A with a 3-day transpacific transport time and plume B with a 5 day transport time. Plume A was injected into the mid-latitude jet in the upper troposphere through deep convection embedded in a mid-latitude cyclone over NE China on 28 June 2004. Plume B was exported in the WCB of a mid-latitude cyclone on 26 June. Note the rapid vertical transport associated with WCB on Figure 5. The upper level geostrophic flow was unusually zonal in the days following injection, favoring very rapid advection across the Pacific with a mean wind speed of 21 m/s and peak winds of 54 m/s (compared to the monthly average of 13 m/s). Both plumes arrived over the NE Pacific on 1 July where they were sampled by the DC-8 aircraft (Figure 4): plume B was intercepted three times (at 36°N, 41°N and 45°N), while plume A was intercepted further south (at 35°N).

Figure 6 shows observed and modeled curtain plots of O_3 along the flight track for 1 July. Figure 7 shows observed vertical profiles of CO, O_3, SO_4^{2-}, HCN and PAN for the same flight. While all five tracers are enhanced in plume B, O_3 and SO_4^{2-} show lower levels and sometimes no enhancement in plume A. This is consistent with the difference in transport time and the more northerly transport of plume A relative to plume B (Figure 5), which would result in less photochemical processing and thus less efficient production of O_3 and SO_4^{2-} for plume A. Indeed, in Plume A CO and O_3 are weakly correlated ($r = 0.20$) with a low O_3-CO slope of 0.17 mol mol^{-1}. CO and O_3 in plume B display a stronger positive correlation ($r = 0.51$) with a high O_3-CO slope of 1.12 mol mol^{-1} (Figure 7c), representing efficient photochemical production of O_3. In addition Table 4 shows that plume B has a lower NO_x/HNO_3 ratio (0.8) compared to plume A (1.2) also consistent with an older plume with more photochemical processing of NO_x to form HNO_3 [*Jaeglé et al.*, 1998].

The 2 August Asian plume was observed over the Gulf of Maine and was the result of intermixing of two Asian plumes. Figure 8 shows the evolution of the plume as observed by MOPITT and modeled by GEOS-Chem. The first plume (plume C) was lifted into the upper troposphere in deep convection over NE China on 24 July 2004 (Figure 8c and 9) and the second plume (plume D) was exported by vigorous lifting in a typhoon to the east of Japan on 28 July 2004 (Figure 8ef and 9). MOPITT CO on 28 July locates plume C in central North Pacific and the edge of Plume D to the east of Japan (Figure 8d). The two plumes merged and advected eastward across the Pacific following the large-scale flow and arrived on the U.S. West Coast on July 31 (Figure 8g-i). The plume was then rapidly transported behind the surface cold front of a mid-latitude cyclone traveling from central Canada to the North Atlantic (Figure 8il). Biomass burning emissions from Alaskan and Canadian fires traveled below the Asian pollution, at 1-4 km, behind the cold front. Enhanced CO levels from these fires can be seen extending from Alaska through Central Canada on both the MOPITT observations and GEOS-Chem simulation on 26, 28 and 31 July (Figure 8). Part of the MOPITT CO column enhancements over the flight track region is due to the transport of these boreal forest fire emissions.

The vertical profiles for the 2 August flight indicate layered influences, as shown on Figure 10. A local pollution layer with moderately high CO mixing ratios was sampled in the boundary layer (0-2 km), extending from New England into the Atlantic. At 2-4 km altitude, co-located CO (> 150 ppbv) and HCN (> 400 ppbv) enhancements indicate the sampling of the biomass burning plume. Finally, in the upper troposphere (8-11 km) the plume with Asian pollution contained elevated CO (100-150 ppbv) , O_3 (60-14 0 ppbv), HCN (320-580 pptv), HNO_3 (up to 1.2 ppbv) and PAN (350-750 pptv). This plume was next to a stratospheric intrusion with high O_3, HNO_3, and low CO.

The chemical characteristics of the two Asian subplumes (C and D) are similar, probably due to the long transport time and sufficient intermixing, we thus do not separate them. The Asian plume of 2 August contained more NO_y (~1590 pptv) compared to the 1 July plume (~880 pptv), consistent with the higher CO levels sampled (Table 4). In this plume the NO_x/HNO_3 ratio is much lower (0.4) compared to the 1 July plumes (1.2 and 0.8), and can be explained by the longer transport time, and thus more conversion of NO_x to HNO_3 in the upper troposphere.

The difference in NO_x levels explains the contrasting levels of H_2O_2 and HNO_4 between the two plumes: 1 July contained high H_2O_2 (~1050 pptv) and low HNO_4 (~64 pptv), while 2 August displayed low H_2O_2 levels (385 pptv) with high HNO_4 (118 pptv). This indicates a shift from a NO_x-limited regime where the main loss of HO_x is via HO_2+HO_2 forming H_2O_2 (1 July), to transition regime with higher NO_x levels (2 August), where $HO_2+NO_2 \rightarrow HNO_4$ competes with the formation of H_2O_2 [*Jaeglé et al.*, 2001; *Kim et al.*, this issue].

CO and O_3 were highly correlated (r = 0.75) in the 2 August Asian plume with a $\Delta O_3/\Delta CO$ ratio of 0.98 mol mol^{-1} (Figure 10b). The high ozone production rate is driven by long transport time, active photochemistry and abundant NO_x.

4.5 Comparison to GEOS-Chem

Simulated concentrations for each airmass type are indicated in parenthesis in Table 2. The model captures reasonably well background levels of O_3, CO, NO_x, PAN, H_2O_2, HCHO, C_2H_6, and C_3H_8, with an overestimate of HNO_3 mixing ratios and underestimate of acetone levels. This is further discussed in *Hudman et al.* [this issue].

Here, we focus on the model's ability to capture the composition of the Asian plumes. While the model captures well the location and timing of the plumes (section 4.1), it underestimates the magnitude of the observed enhancements of O_3 and CO by a factor of 3. Relative to background

levels the mean observed (modeled) enhancements in Asian airmasses are 26 ppbv (8 ppbv) for O_3 and 33 ppbv (11 ppbv) for CO (Table 2). This is also true for individual plumes (see Table 4). In addition, while the observations show a doubling of PAN levels in Asian plumes relative to background, the model shows lower levels of PAN relative to background (Tables 2 and 4). The model also underestimates the observed levels of NO_x in the plumes by a factor of two.

The model's inability to capture the magnitude of observed strong transpacific plumes has been noted previously by *Heald et al.* [2003] and *Hudman et al.* [2004] and was attributed to numerical diffusion in the model. The combined large underestimate of NO_x and PAN that we observe during INTEX-A could be due to a number of additional issues: underestimate of NO_y export from Asia, underestimate of surface NO_x emissions over Asia, and/or and underestimate of lighting over Asia. We examine each of these in turn. Poor representation of the subgrid-scale processes (such as deep convection) could lead to an underestimate of export from Asia. Figure 8 shows that the model significantly underestimates the magnitude of the enhancements observed with MOPITT CO, in particular in the plume associated with export in the typhoon. Using observations from the Global Ozone Monitoring Experiment (GOME), *Richter et al.* [2005] showed that NO_2 columns have increased by 40% over the 1996-2002 period, likely due to growing industrialization and increasing energy consumption. More recently, *Martin et al.* [this issue] derived a new space-based NO_x emissions inventory using SCIAMACHY observations, finding that East Asian emissions in 2004 were 68% larger than the regional bottom-up inventory of *Streets et al.* [2003] for 2000. *Wang et al.* [2003] proposed decomposition of organic wastes and extensive application of chemical fertilizers as a large source of NO_x over Asia. This was confirmed by *Jaeglé et al.* [2005] who found that emissions from soils over Asia account for almost as much NO_x as emissions from anthropogenic combustion sources during summer.

Similar to our systematic model underestimate of Asian influence in the UT, *Wang et al.* [2006] found that global and regional models were not able to capture the late-spring increase in NO_x, PAN, CO, and O_3 observed over North America. They attributed this to a poor representation of convection and lightning over East Asia. It appears that the poor performance of models in capturing the magnitude of transpacific transport enhancements persists though summer.

5. Summary

Several Asian plumes were observed over North America during the NASA INTEX-A aircraft mission during July-August 2004. We applied correlation analysis and Principal Component Analysis (PCA) to the aircraft observations obtained between 6-12 km during INTEX-A to identify Asian plumes in the observations and to examine their composition and origin.

We found distinct influences from Asia (7% of observations), the lower stratosphere (7%), convection and lightning (13%), and boreal forest fires (2%). The remaining 71% are assigned to background. The Asian airmasses are significantly enhanced in CO, O_3, PAN, HCN, C_2H_2, benzene, and SO_4^{2-}, consistent with the dominant influence of combustion emissions over East Asia. In addition, high levels of methanol and acetone indicate that biogenic emissions combine with the polluted outflow.

Our observations-based PCA method identifies five major Asian pollution plumes during INTEX-A. The Asian origin of these plumes is confirmed with results from the GEOS-Chem global model of tropospheric chemistry as well as back trajectories. The three main summertime trans-Pacific transport mechanisms are export of Asian pollution in the warm conveyor belts of

the mid-latitude cyclones, deep convection, and lifting in typhoons followed by advection in the middle and upper troposphere for 3-9 days. Individual Asian plumes have some common characteristics (elevated CO, PAN, HCN, C_2H_2, and methanol), but differ in the amounts of O_3, HNO_3, and SO_4^{2-} present. We explain the differences in terms of a range of chemical processing time and aging of the polluted airmasses with conversion of NO_x to HNO_3 accompanied by efficient O_3 production.

We contrast the composition of these summertime Asian plumes to observations obtained during spring: PEM-West B, PHOBEA, TRACE-P, and ITCT2K2. INTEX-A plumes contain lower levels of anthropogenic pollutants because of their shorter lifetime during summer. They display higher levels of biogenic tracers, indicating a more active biosphere. Finally, the Asian plumes observed during INTEX-A contain higher levels of reactive nitrogen species and O_3, likely the result of active photochemistry fueled by higher NO_x export from the Asian boundary layer. Additional summertime injection of lightning NO_x over East Asia or the western Pacific might have further enhanced reactive nitrogen levels in the upper troposphere. Stratosphere-troposphere exchange along isentropes accounts for part of the observed O_3 enhancements.

Although the GEOS-Chem model captures the timing and location of the observed Asian plumes, it underestimates the magnitude of enhancements of CO and O_3 by a factor of 3. In addition, the model does not show any enhancements in PAN (observations show a doubling relative to background levels) and significantly underestimates NO_x levels in the plumes. While some of these underestimates are likely due to transport problems (numerical diffusion and poor representation of subgridscale features such as deep convection), it is also likely that the model underestimates surface NO_x emissions over Asia and/or lightning emissions over Asia.

Acknowledgements.
This work was supported by funding from NASA and NSF (ATM 0238530). The GEOS-Chem model is managed by the Atmospheric Chemistry Modeling group at Harvard University with support from the NASA Atmospheric Chemistry Modeling and Analysis Program.

References.

Alexander B., R. J. Park, D. J. Jacob, Q. B. Li, R. M. Yantosca, J. Savarino, C. C. W. Lee, M. H. Thiemens (2005), Sulfate formation in sea-salt aerosols: Constraints from oxygen isotopes, *J. Geophys. Res., 110*, D10307, doi:10.1029/2004JD005659.

Al-Saadi, J., et al., Lagrangian Characterization of the Sources and Chemical Transformation of Air Influencing the Continental US during the 2004 ICARTT/INTEX-A Campaign, *J. Geophys. Res.,* this issue.

Andreae, M. O., H. Berresheim, T. W. Andreae, M. A. Kritz, T. S. Bates, and J. T. Merrill (1988), Vertical distribution of dimethylsulfide, sulfur dioxide, aerosol ions, and radon over the northeast Pacific Ocean, *J. Atmos. Chem., 6,* 149-173.

Avery et al.,

Bartlett, K. B., G. W. Sachse, T. Slate, C. Harward, and D. R. Blake (2003), Large-scale distribution of CH_4 in the western North Pacific: Sources and transport from the Asian continent, *J. Geophys. Res.*, 108(D20), 8807, doi:10.1029/2002JD003076.

Berntsen, T. K., S. Karlsdottir, and D. A. Jaffe (1999), Influence of Asian emissions on the composition of air reaching the North Western United States, *Geophys. Res. Lett., 26,* 2171-2174 .

Bertschi I. T., D. A. Jaffe, L. Jaeglé, H. U. Price, J. B. Dennison (2004), PHOBEA/ITCT 2002 airborne observations of transpacific transport of ozone, CO, volatile organic compounds, and aerosols to the northeast Pacific: Impacts of Asian anthropogenic and Siberian boreal fire emissions, *J. Geophys. Res., 109*, D23S12, doi:10.1029/2003JD004328.

Bey, I., D. J. Jacob, R. M. Yantosca, J. A. Logan, B. D. Field, A. M. Fiore, Q. Li, H. Y. Liu, L. J. Mickley, and M. G. Schultz (2001a), Global modeling of tropospheric chemistry with assimilated meteorology: Model description and evaluation, *J. Geophys. Res., 106,* 23,073-23096.

Bey, I., D. J. Jacob, J. A. Logan, R. M. Yantosca (2001b), Asian chemical outflow to the Pacific: Origins, pathways and budgets, *J. Geophys. Res., 106*, 23,097-23,114.

Blake, D. R., T. Y. Chen, T. W. Smith, C. J. L. Wang, O. W. Wingenter, N. J. Blake, F. S. Rowland, E. W. Mayer (1996), Three-dimensional distribution of nonmethane hydrocarbons and halocarbons over the northwestern Pacific during the 1991 Pacific Exploratory Mission (PEM-West A), *J. Geophys. Res., 101*, 1763-1778.

Blake, N., et al., (2003), NMHCs and halocarbons in Asian continental outflow during TRACE-P: Comparison to PEM-West B, *J. Geophys. Res., 108*(D20), 8806, doi:10.1029/2002JD003367.

Brock C. A., et al. (2004), Particle characteristics following cloud-modified transport from Asia to North America, *J. Geophys. Res.*, 109, D23S26, doi:10.1029/2003JD004198.

Browell, E. V., et al. (2003), Large-scale ozone and aerosol distributions, air mass characteristics, and ozone fluxes over the western Pacific Ocean in late winter/early spring, *J. Geophys. Res., 108*(D20), 8805, doi:10.1029/2002JD003290.

Brune, et al., HOx chemistry and ozone production in the different plumes during INTEX-A, *J. Geophys. Res.,* this issue.

Buhr, M., D. Parrish, J. Elliot, J. Holloway, J. Carpenter, P. Goldan, W. Kuster, M. Trainer, S. Montzka, S. Mckeen, and F. Fehsenfeld (1995), Evaluation of ozone precursor source types using principal component analysis of ambient air measurements in rural Alabama, *J. Geophys. Res.*, 100, 22,853-22,860.

Clarke, A. D., et al. (2002) The INDOEX aerosol: A comparison and summary of microphysical, chemical, and optical properties observed from land, ship, and aircraft, *J. Geophys. Res., 107*(D19), 8033, doi:10.1029/2001JD000572.

Cofer, W. R.; Winstead, E. L.; Stocks, B. J.; Goldammer, J. G.; Cahoon, D. R. (1998), Crown fire emissions of CO_2, CO, H_2, CH_4, and TNMHC from a dense jack pine boreal forest fire, *Geophys. Res. Lett., 25*, 3919-3922.

Cohen, R. C., et al., (2000), Quantitative constraints on the atmospheric chemistry of nitrogen oxides: An analysis along chemical coordinates, *J. Geophys. Res., 105*(D19), 24283-24304, 10.1029/2000JD900290.

Crawford, J. H., et al. (2003), Clouds and trace gas distributions during TRACE-P, *J. Geophys. Res., 108*(D21), 8818, doi:10.1029/2002JD003177.

Crounse, J., P. Wennberg, Kwan, B. Heikes, O'Sullivan, Shen, J. H. Crawford, Peroxyacetic acid is ubiquitous in the upper troposphere, *J. Geophys. Res.,* this issue.

Deeter, M. N., et al. (2003), Operational carbon monoxide retrieval algorithm and selected results for the MOPITT instrument, *J. Geophys. Res., 108* (D14), 4399, doi:10.1029/2002JD003186.

Deeter, M. N., et al. (2004), Evaluation of operational radiances for the Measurements of Pollution in the Troposphere (MOPITT) instrument CO thermal band channels, *J. Geophys. Res., 109*, D03308, doi:10.1029/2003JD003970.

Drummond, J. R., and G.S. Mand (1996), The Measurements of Pollution in the Troposphere (MOPITT) instrument: Overall performance and calbration requirements, *J. Atmos. Oceanic. Technol*., 13, 314-320.

de Gouw J. A., C. Warneke, D. D. Parrish, J. S. Holloway, M. Trainer, F. C. Fehsenfeld (2003), Emission sources and ocean uptake of acetonitrile (CH_3CN) in the atmosphere, *J. Geophys. Res., 108* (D11), 4329, doi:10.1029/2002JD002897.

de Gouw J. A., et al. (2004), Chemical composition of air masses transported from Asia to the U.S. West Coast during ITCT 2K2: Fossil fuel combustion versus biomass-burning signatures, *J. Geophys. Res., 109*, D23S20, doi:10.1029/2003JD004202.

Dibb, J. E., R. W. Talbot, E. Scheuer, G. Seid, L. DeBell, B. Lefer, and B. Ridley (2003a), Stratospheric influence on the northern North American free troposphere during TOPSE: ^{7}Be as a stratospheric tracer, *J. Geophys. Res., 108*(D4), 8363, doi:10.1029/2001JD001347.

Dibb J. E., R. W. Talbot, E. M. Scheuer, G. Seid, M. A. Avery, H. B. Singh (2003b), Aerosol chemical composition in Asian continental outflow during the TRACE-P campaign: Comparison with PEM-West B, *J. Geophys. Res., 108*(D21), 8815, doi:10.1029/2002JD003111.

Duncan, B. N., et al. (2003), Interannual and Seasonal Variability of Biomass Burning Emissions Constrained by Satellite Observations, *J. Geophys. Res.*, *108*, doi:10.1029/2002JD002378.

Duncan, B. N., and I. Bey (2004), A modeling study of the export pathways of pollution from Europe: Seasonal and interannual variations (1987–1997), *J. Geophys. Res., 109*, D08301, doi:10.1029/2003JD004079.

Fairlie, T. D., D. J. Jacob, and R. J. Park (2006), The impact of transpacific transport of mineral dust in the United States, submitted to *Atmos. Environ*.

Fiore, A. M., D. J. Jacob, I. Bey, R. M. Yantosca, B. D. Field, and A. C. Fusco (2002), Background ozone over the United States in summer: Origin, trend, and contribution to pollution episodes, *J. Geophys. Res., 107*(D15), doi:10.1029/2001JD000982.

Fried, A., et al. (2003), Airborne tunable diode laser measurements of formaldehyde during TRACE-P: distributions and box-model comparisons, *J. Geophys. Res., 108*(D20), 8798, doi:10.1029/2003JD003451.

Fuelberg H. E., C. M. Kiley, J. R. Hannan, D. J. Westberg, M. A. Avery, R. E. Newell (2003), Meteorological conditions and transport pathways during the Transport and Chemical Evolution over the Pacific (TRACE-P) experiment, *J. Geophys. Res., 108* (D20), 8782, doi:10.1029/2002JD003092.

Fuelberg, H. E, M. Porter, C. M. Kiley, D. Morse, A meteorological overview of the INTEX-A period, *J. Geophys. Res.,*this issue.

Goode, J. G., R. J. Yokelson, D. E. Ward, R. A. Susott, R. E. Babbitt, M. A. Davies, W. M. Hao (2000), Measurements of excess O_3, CO_2, CH_4, C_2H_4, C_2H_2, HCN, NO, NH_3, HCOOH, CH_3COOH, HCHO, and CH_3H in 1997 Alaskan biomass burning plumes by airborne Fourier transform infrared spectroscopy (AFTIR) [O_3 CO_2 CH_4 C_2H_4 C_2H_2 NH_3 CH_3COOH CH_3H], *J. Geophys. Res., 105*, 22,147-22,166.

Guo, H., T. Wang, and P. K. K. Louie (2004), Source apportionment of ambient non-methane hydrocarbons in Hong Kong: Application of a principal component analysis/absolute principal component scores (PCA/APCS) receptor model, *Environ. Pollut., 129*, 489-498.

Heald, C. L., D. J. Jacob, P. I. Palmer, M. J. Evans, G. W. Sachse, H. B. Singh, D. R. Blake (2003), Biomass burning emission inventory with daily resolution: Application to aircraft observations of Asian outflow, *J. Geophys. Res., 10* (D21), 8811, doi:10.1029/2002JD003082.

Heald, C. L., D. J. Park, B. Alexander, T. D. Fairlie, D. a. Chu, R. M. Yantosca (2006), Transpacific transport of anthropogenic aerosols and its impact on surface air quality in the United States, submiteed to *J. Geophys. Res.*

Heikes, B. G., et al. (1996), Hydrogen peroxide and methylhydroperoxide distributions related to ozone and odd hydrogen over the North Pacific in the fall of 1991, *J. Geophys. Res., 101*(D1), 1891-1906, 10.1029/95JD01364.

Heikes, B.G., et al. (2002), Atmospheric methanol budget and ocean implications, *Glob. Biogeochem. Cycl.*, 16(4), 1133, doi:10.1029/2002GB001895.

Hoell, J. M., D. D. Davis, S. C. Liu, R. E. Newell, H. Akimoto, R. J. McNeal, R. J. Bendura (1997), The Pacific Exploratory Mission-West Phase B: February - March, 1994, *J. Geophys. Res., 102*(D23), 28223-28240, 10.1029/97JD02581.

Holzer, M., T. M. Hall, R. B. Stull (2005), Seasonality and weather-driven variability of transpacific transport, J. Geophys. Res., 110, D23103, doi:10.1029/2005JD006261.

Hudman, R. C., et al. (2004), Ozone production in transpacific Asian pollution plumes and implications for ozone air quality in California, *J. Geosphys. Res., 109,* D23S18, doi:10.1029/2004JD004978.

Hudman, R. C., et al., A multi-platform analysis of the North American reactive nitrogen budget during the ICARTT summer intensive, *J. Geophys. Res.,* this issue.

Huey, L. G., et al (2004), CIMS measurements of HNO_3 and SO_2 at the South Pole during ISCAT 2000, *Atmos. Environ., 38* (32) 5411-5421.

Husar, R. B., et al. (2001), The Asian dust events of April 1998, *J. Geophys. Res., 106,* 18,317-18,333.

Jacob, D. J., J. A., Logan, and P. P. Murti (1999), Effect of rising Asian emissions on surface ozone in the United States, *Geophys. Res. Lett., 26,* 2175-2178.

Jacob, D. J., J. H. Crawford, M. M. Kleb, V. S. Connors, R. J. Bendura, J. L. Raper, G. W. Sachse, J. C. Gille, L. Emmons, C. L. Heald (2003), Transport and Chemical Evolution over

the Pacific (TRACE-P) aircraft mission: Design, execution, and first results, *J. Geophys. Res., 108*(D20), 9000, doi:10.1029/2002JD003276.

Jacob, D. J., B. D. Field, Q. Li, D. R. Blake, J. de Gouw, C. Warneke, A. Hansel, A. Wisthaler, and H. B. Singh (2005), Global budget of methanol: constraints from atmospheric observations, *J. Geophys. Res., 110*, D08303, doi:10.1029/2004JD005172.

Jaeglé, L., et al. (1998) Sources and chemistry of NO_x in the upper troposphere over the United States, Geophys. Res. Lett., 25, 1705-1708.

Jaeglé, L., D. J. Jacob, W. H. Brune, and P. O. Wennberg (2001), Chemistry of HO_x radicals in the upper troposphere, *Atmos. Env*., 35, 469-489.

Jaeglé, L., D. Jaffe, H. U. Price, P. Weiss-Penzias, P. I. Palmer, M. J. Evans, D. J. Jacob, I. Bey (2003), Sources and Budgets for CO and O_3 in the Northeastern Pacific during the spring of 2001: Results from the PHOBEA-II Experiment, *J. Geophys. Res., 108*(D20), 8802, doi:10.1029/2002JD003121.

Jaeglé, L., L., Steinberger, L., R. V. Martin, and K.Chance (2005), Global partitioning of NO_x sources using satellite observations: Relative roles of fossil fuel combustion, biomass burning and soil emissions, *Faraday Discuss.* 130, 407−423, doi:10.1039/b502128f.

Jaffe, D. A., et al. (1999), Transport of Asian air pollution to North America, *Geophys. Res. Lett., 26*, 711-714.

Jaffe, D.A., T. Anderson, D. Covert, B. Trost, J. Danielson, W. Simpson, D. Blake, J. Harris, and D. Streets (2001), Observations of ozone and related species in the Northeast Pacific during the PHOBEA Campaigns: 1. Ground based observations at Cheeka Peak, *J. Geophys. Res., 106,* 7449-7461.

Jaffe, D.A., I. McKendry, T. Anderson, and H. Price (2003), Six new episodes of trans-Pacific transport of air pollutants, *Atmos. Environ., 37,* 391-404 .

Jaffe, D., I. Bertschi, L. Jaegle, P. Novelli, J. S. Reid, H. Tanimoto, R. Vingarzan, and D. L. Westphal (2004), Long-range transport of Siberian biomass burning emissions and impact on surface ozone in western North America, *Geophys. Res. Lett., 31*, L16106, doi:10.1029/2004GL020093.

Jing, P., D. M. Cunnold, H. J. Wang, and E.-S. Yang (2004), Isentropic Cross-Tropopause Ozone Transport in the Northern Hemisphere, *J. Atmos. Sci., 61*, 1068-1078.

Kim, S., et al., Measurements of HO_2NO_2 in the Upper troposphere during INTEX-A *J. Geophys. Res.,* this issue.

Kline J., B. Huebert, S. Howell, B. Blomquist, J. Zhuang, T. Bertram, J. Carrillo (2004), Aerosol composition and size versus altitude measured from the C-130 during ACE-Asia, *J. Geophys. Res., 109*, D19S08, doi:10.1029/2004JD004540.

Kotchenruther, R. A., D. A. Jaffe, H. J. Beine, T. L. Anderson, J. W. Bottenheim, J. M. Harris, D. R. Blake, and R. Schmitt (2001), Observations of ozone and related species in the northeastern Pacific during the PHOBEA campaign: 2. Airborne observations, *J. Geophys. Res., 106,* 7463-7483.

Kritz, M. A., J. C. LeRoully, and E. F. Danielson (1990), The China Clipper: Fast advective transport of radon-rich air from the Asian boundary layer to the upper troposphere near California, *Tellus, 4213,* 46-61.

Lelieveld J., W. Peters, F. J. Dentener, and M. C. Krol (2002), Stability of tropospheric hydroxyl chemistry, J. Geophys. Res., 107 (D23), 4715, doi:10.1029/2002JD002272.

Li, Q., et al. (2002), Transatlantic transport of pollution and its effects on surface ozone in Europe and North America, *J. Geophys. Res., 107*(D13), doi:10.1029/2001JD001422.

Li, Q., D. J. Jacob, R. Yantosca, C. Heald, H. Singh, M. Koike, Y. Zhao, G. W. Sachse, and D. Streets (2003), A global three-dimensional model analysis of the atmospheric budgets of HCN and CH_3CN: constraints from aircraft and ground measurements, *J. Geophys. Res., 108*(D21), 8827, doi:10.1029/2002JD003075.

Li, Q., D. J. Jacob, J. W. Munger, R. M. Yantosca, D. D. Parrish (2004), Export of NOy from the North American boundary layer: Reconciling aircraft observations and global model budgets, *J. Geophys. Res., 109*, D02313, doi:10.1029/2003JD004086.

Li, Q. B., D. J. Jacob, R. Park, Y. Wang, C. L. Heald, R. Hudman, R.M. Yantosca, R.V. Martin, and M.Evans (2005), North American pollution outflow and the trapping of convectively lifted pollution by upper-level anticyclone, *J. Geophys. Res., 110*, D10301, doi:10.1029/2004JD005039.

Li, Y., J. Staehelin, M. Auvray, I. Bey, and M. Schultz (2006), Comparison between numerical simulations of two 3-D global models (GEOS-Chem and MOZART) with ozone observations atJungfraujoch (Switzerland) and ozone sondes from Payerne, submitted to *Atmos. Environ.*.

Liang, Q., L. Jaeglé, D. A. Jaffe, P. Weiss-Penzias, and A. Heckman (2004), Long-range transport of Asian pollution to the northeast Pacific: Seasonal variations and transport pathways of carbon monoxide, *J. Geophys. Res., 109,* D23S07, doi:10.1029/2003JD4402.

Liang, Q., L. Jaeglé, and J. M. Wallace (2005), Meteorological Indices for Asian Outflow and Transpacific Transport on Daily to Interannual Timescales, *J. Geophys. Res., 110,* D18308, doi:10.1029/2005JD005788.

Lin, C., and A. Arakawa (2000), Empirical Determination of the Basic Modes of Cumulus Heating and Drying Profiles, *J. Atmos. Sci.,* 57, 3571-3591.

Liu H., D. J. Jacob, L. Y. Chan, S. J. Oltmans, I. Bey, R. M. Yantosca, J. M. Harris, B. N. Duncan, and R. V. Martin (2002), Sources of tropospheric ozone along the Asian Pacific Rim: An analysis of ozonesonde observations, *J. Geophys. Res., 107* (D21), 4573, doi:10.1029/2001JD002005.

Liu, H., D. J. Jacob, I. Bey, R. M. Yantosca, B. N. Duncan, G. W. Sachse (2003), Transport pathways for Asian pollution outflow over the Pacific: Interannual and seasonal variations, *J. Geophys. Res., 108*(D20), 8786, doi:10.1029/2002JD003102.

Martin, R. V., et al. (2002), Interpretation of TOMS observations of tropical tropospheric ozone with a global model and in-situ observations, *J. Geophys. Res., 107*(D18), 4351, doi:10.1029/2001JD001480.

Martin, R. V., et al., Evaluation of space-based constraints on nitrogen oxide emissions with regional aircraft measurements over and downwind of eastern North America, *J. Geophys. Res.,* this issue.

Mauzerall, D. L., D. Narita, H. Akimoto, L. Horowitz, S. Walters, D. A. Hauglustaine, G. Brasseur (2000), Seasonal characteristics of tropospheric ozone production and mixing ratios over East Asia: A global three-dimensional chemical transport model analysis, *J. Geophys. Res., 105*(D14), 17895-17910, 10.1029/2000JD900087.

Merrill, J. T., M. Uematsu, and R. Bleck (1989), Meteorological analysis of long range transport of mineral aerosol over the North Pacific, *J. Geophys. Res., 94,* 8584-8598.

Millet, D. B., et al., Formaldehyde distribution over North America: Implications for satellite retrievals of formaldehyde columns and isoprene emission, *J. Geophys. Res.,* this issue.

Morris, G. A., et al., Alaskan and Canadian forest fires exacerbate ozone pollution over Houston, Texas, on 19 and 20 July 2004, *J. Geophys. Res.,* this issue.

Newell, R. E., et al. (1996), Atmospheric sampling of Supertyphoon Mireille with NASA DC-8 aircraft on September 27, 1991, during PEM-West A, *J. Geophys. Res., 101,* 1853-1872.

Nowak, J. B., et al. (2004), Gas-phase chemical characteristics of Asian emission plumes observed during ITCT 2K2 over the eastern North Pacific Ocean, *J. Geophys. Res.*, *109*, D23S19, doi:10.1029/2003JD004488.

Palmer, P. I., D. J. Jacob, A. M. Fiore, R. V. Martin, K. Chance, and T. P. Kurosu (2003), Mapping isoprene emissions over North America using formaldehyde column observations from space, *J. Geophys. Res., 108*(D6), 4180, doi:10.1029/2002JD002153.

Park, R. J., D. J. Jacob, M. Chin, R. V. Martin (2003), Sources of carbonaceous aerosols over the United States and implications for natural visibility, *J. Geophys. Res., 108*(D12), 4355, doi:10.1029/2002JD003190.

Park, R. J., D. J. Jacob, B. D. Field, R. M. Yantosca, and M. Chin (2004), Natural and transboundary pollution influences on sulfate-nitrate-ammonium aerosols in the United States: implications for policy, *J. Geophys. Res.,* 109, D15204, doi:10.1029/2003JD004473.

Parrish, D. D., C. J. Hahn, E. J. Williams, R. B. Norton, F. C. Fehsenfeld, H. B. Singh, J. D. Shetter, . W. Gandrud, and B. A. Ridley (1992), Indications of photochemical histories of Pacific air masses from measurements of atmospheric trace species at Pt. Arena, California, *J. Geophys. Res., 97,* 15,883-15,901.

Parrish, D. D., Y. Kondo, O. R. Cooper, C. A. Brock, D. A. Jaffe, M. Trainer, T. Ogawa, G. Hübler, and F. C. Fehsenfeld (2004), Intercontinental Transport and Chemical Transformation 2002 (ITCT 2K2) and Pacific Exploration of Asian Continental Emission (PEACE) experiments: An overview of the 2002 winter and spring intensives, *J. Geophys. Res.*, *109*, D23S01, doi:10.1029/2004JD004980.

Pfister, G., P. G. Hess, L. K. Emmons, J.-F. Lamarque, C. Wiedinmyer, D. P. Edwards, G., Pétron, J. C. Gille, and G. W. Sachse (2004), Quantifying CO emissions from the 2004 Alaskan wildfires using MOPITT CO data, *Geophys. Res. Lett., 32,* L11809, doi:10.1029/2005GL022995.

Price H. U., D. A. Jaffe, P. V. Doskey, I. McKendry, T. L. Anderson (2003), Vertical profiles of O3, aerosols, CO and NMHCs in the Northeast Pacific during the TRACE-P and ACE-ASIA experiments, *J. Geophys. Res., 108* (D20), 8799, doi:10.1029/2002JD002930.

Price, H. U., D. A. Jaffe, O. R. Cooper, and P. V. Doskey (2004), Photochemistry, ozone production, and dilution during long-range transport episodes from Eurasia to the northwest United States, *J. Geophys. Res., 109*, D23S13, doi:10.1029/2003JD004400.

Richter,A.*, et al* (2005), Increase in tropospheric nitrogen dioxide over China observed from space, *Nature*, 437, 129-132.

Scott, R. K.， and J.-P. Cammas (2002): Wave breaking and mixing at the subtropical tropopause, *J. Atmos. Sci., 59,* 2347-2361.

Singh, H. B., M. Kanakidou, P. J. Crutzen, and D. J. Jacob (1995), High concentrations and photochemical fate of oxygenated hydrocarbons in the global troposphere, Nature, 378, 50-54.

Singh, H. B., et al. (2000), Distribution and fate of selected oxygenated organic species in the troposphere and lower stratosphere over the Atlantic, *J. Geophys. Res.*, 105, 3795-3806.

Singh, H. B., et al. (2003), In situ measurements of HCN and CH_3CN over the Pacific Ocean: Sources, sinks, and budgets, *J. Geophys. Res., 108*(D20), 8795, doi:10.1029/2002JD003006.

Singh, H. B., et al. (2004), Analysis of the atmospheric distribution, sources, and sinks of oxygenated volatile organic chemicals based on measurements over the Pacific during TRACE-P, *J. Geophys. Res., 109*, doi:10.1029/2003JD003883.

Singh, H. B., W. Brune, J. Crawford, and D. Jacob, Overview of the Summer 2004 Intercontinental Chemical Transport Experiment-North America (INTEXA), *J. Geophys. Res.,* this issue.

Statheropoulos, M., N. Vassiliadis, and A. Pappa (1998), Principal component and canonical correlation analysis for examining air pollution and meteorological data, *Atmos. Environ.*, 32, 1087-1095.

Stohl, A. (2001), A 1-year lagrangian climatology of airstreams in the Northern Hemisphere troposphere and lowermost stratosphere, *J. Geophys. Res., 106*, 7263-7279.

Stohl, A., S. Eckhardt, C. Forster, P. James, and N. Spichtinger (2002), On the pathways and timescales of intercontinental air pollution transport, *J. Geophys. Res., 107*(D23), 4684, doi:10.1029/2001JD001396.

Streets D. G., et al. (2003), An inventory of gaseous and primary aerosol emissions in Asia in the year 2000, *J. Geophys. Res., 108* (D21), 8809, doi:10.1029/2002JD003093.

Thurston, G. D., and J. D. Spengler (1985), A quantitative assessment of source contributions to inhalable particulate matter pollution in metropolitan Boston *Atmos. Environ.*, 19, 9-26.

Turquety, S., et al. Inventory of boreal fire emissions for North America: important of pear burning and pyro-convective injection, *J. Geophys. Res.,* this issue.

Wang, Y., J. A. Logan, D. J. Jacob (1998), Global simulation of tropospheric O 3 -NOx-hydrocarbon chemistry 2. Model evaluation and global ozone budget, *J. Geophys. Res., 103*(D9), 10727-10756, 10.1029/98JD00157.

Wang Y., et al. (2003), Springtime photochemistry at northern mid and high latitudes, *J. Geophys. Res., 108* (D4), 8358, doi:10.1029/2002JD002227.

Wang, Y., Y. Choi, T. Zeng, B. Ridley, N. Blake, D. Blake, F. Flocke (2006), Late-spring increase of trans-Pacific pollution transport in the upper troposphere, *Geophys. Res. Lett., 33,* L01811, doi:10.1029/2005GL024975.

Weiss-Penzias, P., D. A. Jaffe, A. Heckman, L. Jaeglé, and Q. Liang (2004), The influence of long-range transported pollution on the annual and diurnal cycles of carbon monoxide and ozone at Cheeka Peak Observatory, *J. Geophys. Res., 109,* D23S14, doi:10.1029/2004JD004505.

Yevich, R., and J. A. Logan (2003), An assessment of biofuel use and burning of agricultural waste in the developing world, *Global Biogeochem. Cycles, 17*(4), 1095, doi:10.1029/2002GB001952.

Yienger, J. J., M. Galanter, T. A. Holloway, M. J. Phadnis, S. K. Guttikunda, C. R. Carmichael, W. J. Moxim, and H. Levy II (2000), The episodic nature of air pollution transport from Asia to North America, *J. Geophys. Res., 105*, 26,931-26,945.

Yienger, J. J., and H. Levy (1995), Empirical model of global soil-biogenic NO_x emissions, *J. Geophys. Res., 100*(D6), 11447-11464, 10.1029/95JD00370.

Zhang, L., et al. (2006), Continental outflow of ozone pollution as determined by O_3-CO correlations from the TES satellite instrument, *Geophys. Res. Lett*, submitted.

Figure captions.

Figure 1. Structure of the 3 leading Empirical Orthogonal Functions (EOF) identified by Principal Component Analysis applied to observations between 6 -12 km.

Figure 2. Scatter diagram of observed (a) 10-sec CO and O_3, (b) 75-sec CO and PAN, and (c) 6.5-sec CO and HNO_3, (d) 2-min CO and SO_4^{2-}, (e) 10-sec CO and HCN, (f) 1-min CO and acetylene, (g) 1-min O_3 and NO_y ($NO_y = NO + NO_2 + PAN + HNO_3 + HNO_4$), (h) 1-min CO and NO_y within different airmasses between 6-12 km during INTEX-A. Biomass burning plumes that have CO > 200 ppbv are not shown here.

Figure 3. Flight tracks of the NASA DC-8 aircraft during INTEX-A (July 1 – August 14, 2004). Filled circles indicate locations of Asian plumes identified using (a) Principal Component Analysis, (b) the GEOS-Chem Asian CO tracer, and (c) FSU back trajectories, size-scaled and color-scaled according to the observed CO levels.

Figure 4. G GEOS-Chem Asian CO tracer for the INTEX-A flight on 1 July, 2004. Panel a): Asian CO at 369 hPa (8.8 km) with the DC-8 flight track marked by the write thick line. Locations where plume A and B were sampled were highlighted in red and blue, respectively. Panel b): Curtain plot of Asian CO along the flight track. The black circles with letter "A" and "B" indicate plumes A and B, respectively.

Figure 5. Kinematic back trajectories for the 1 July 2004 Asian plume: 3 day back trajectories for plume A are shown in red and 5 day back-trajectories for plume B are shown in blue. The thick black line indicates the flight track.

Figure 6. Curtain plots of (a) observed in situ O_3, (b) DIAL O_3, and (c) model O_3 along the 1 July 2004 flight track. The black circles with letter "A" and "B" indicate plumes A and B, respectively.

Figure 7. Vertical profiles of observed CO, O_3, HCN, PAN, and fine sulfate aerosols during the 1 July 2004 flight are shown in panels a-b and d-f. Thick gray lines are the mean observed vertical profiles in background air. Scatter plot of CO versus O_3 is in panel c. The two Asian sub-plumes are highlighted in color: plume A in blue and plume B in red.

Figure 8. MOPITT CO at 350 hPa (left panels), GEOS-Chem CO (with MOPITT kernel applied) at 350 hPa (middle panels), and GEOS-Chem Asian CO (right panels) at 369 hPa for 26 July, 28 July, 31 July, and 2 August 2004. MOPITT CO is regridded to the model resolution for comparison. Sea level pressure (contours) are also overplotted on the model CO. The white thick line on panel (j) indicates the flight track. The circles and letter "C" and "D" indicates the location of subplumes C and D, respectively.

Figure 9. 8 day back trajectories for the 2 August Asian plume. The thick black line indicates the flight track.

Figure 10. Observed vertical profile of CO, O_3, HCN, and HNO_3 between 14 – 16.4 UTC during the 2 August 2004 flight are shown in panels a and c - e. Note the change in the scale of x-axis in panel c from 0-150 ppbv to 150-400 ppbv. Thick gray lines are the mean observed vertical profiles in background air. Scatter plot of CO versus O_3 is in panel b. The Asian plume is highlighted in blue.

Table 1. Summary of in situ observations.

Species	Instrument & Methods	Reference
CO, CH_4	Diode laser spectrometer	*Bartlett et al.* [2003]
O_3	Nitric oxide chemiluminescence	*Avery et al.* [this issue]
HNO_3	i) Chemical Ionization Mass Spectrometer (CIMS) ii) Sample collected by mist chamber and later analyzed by ion chromatography	i) *Crounse et al.* [this issue] ii) *Dibb et al.* [2003a]
PAN	Automated dual gas chromatography with cryofocusing	*Singh et al.* [2004]
NO	Chemiluminescence analyzer	*Brune et al.* [this issue]
OH, HO_2	Laser induced fluorescence	*Brune et al.* [this issue]
NO_2, PNs	Laser induced fluorescence	*Cohen et al.* [2000]
H_2O_2	i) CMIS ii) Aqueous collection followed by high pressure liquid chromatography (HPLC) separation and enzyme fluorescence detection	i) *Crounse et al.* [this issue] ii) *Heikes et al.* [1996]
CH_3OOH	Aqueous collection followed by high pressure liquid chromatography (HPLC) separation and enzyme fluorescence detection	*Heikes et al.* [1996]
HNO_4, SO_2	CIMS	*Huey et al.* [2004]
HCHO	tunable diode laser absorption spectroscopic (TDLAS)	*Fried et al.* [2003]
Acetone, acetyldehyde	Photo ionization detector	*Singh et al.* [2004]
Methanol, ethanol, CH_3CN, HCN	Reduction gas detector	*Singh et al.* [2004]
Ethane, ethane, acetylene, propane benzene, toluene, CFC-11, CFC-12, CFC-113, H-1211	Sample analyzed with gas chromatography/mass spectrometry (GC/MS)	*Blake et al.* [2003]
Condensation Nuclei	TSI Condensation Particle Counter	*Clarke et al.* [2002]
^7Be	Sample collected by Teflon filters and analyzed using gamma-spectroscopy and alpha-spectroscopy	*Dibb et al.* [2003b]
NO_3^-, SO_4^{2-}, $C_2O_4^{2-}$, NH^{4+}, Na^+, K^+, Mg^{2+}, Ca^{2+}	Sample collected by Teflon filters and later extracted into deionized water with ion chromatography analysis performed.	*Dibb et al.* [2003b]
Fine sulfate aerosols	Sample collected by mist chamber and analyzed by ion chromatography.	*Dibb et al.* [2003b]

Table 2. Observed chemical composition of airmasses sampled at 6-12 km.

	Background	**EOF 1** Lower Stratosphere	**EOF 2** Convection & Lightning	**EOF 3** Asian	Biomass Burning
Number of 1-min measurements	2580	243	482	255	73
O_3, ppbv	73 ± 17 (75)	**212 ± 85 (92)**	78 ± 20 (80)	**99 ± 20** (83)	74 ± 19 (68)
CO, ppbv	95 ± 15 (94)	80 ± 23 (92)	103 ± 18 (92)	**128 ± 14** (106)	**255 ± 154 (130)**
H_2O, ppmv	719 ± 880	89 ± 101	231 ± 181	527 ± 428	419 ± 345
Relative humidity, %	48.5 ± 26.8	23.7 ± 19.9	60.2 ± 23.9	52.0 ± 25.3	33.6 ± 11.5
NO_x[a], pptv	285 ± 223 (210)	327 ± 177 (140)	**1041 ± 603** (437)	289 ± 201 (130)	227 ± 158 (67)
PAN, pptv	301 ± 163 (296)	279 ± 152 (183)	398 ± 216 (262)	**592 ± 159** (275**)**	**1033 ± 653** (281)
ΣPNs[b], pptv	295 ± 193	338 ± 219	394 ± 289	491 ± 194	**1188 ± 840**
HNO_3, pptv	245 ± 210 (416)	**677 ± 340** (294)	209 ± 175 (435)	363 ± 304 (279)	367 ± 234 (128)
HNO_4, pptv	53 ± 34	83 ± 33	65 ± 33	86 ± 44	86 ± 40
NO_y[c], pptv	884 ± 436 (963)	**1366 ± 359** (624)	**1713 ± 867** (1019)	**1330 ± 458** (527)	**1713 ± 827** (476)
NO_x/HNO_3 (pptv/pptv)	0.38 ± 0.32	0.26 ± 0.21	**1.26 ± 0.93**	0.30 ± 0.24	0.29 ± 0.34
SO_2, pptv	33 ± 45 (17)	33 ± 27 (27)	51 ± 79 (15)	38 ± 25 (18)	22 ± 11 (30)
HCN, pptv	285 ± 67	314 ± 86	301 ± 77	**420 ± 60**	**1085 ± 854**
CH_3CN, ppptv	147 ± 23	149 ± 29	145 ± 23	159 ± 30	**553 ± 396**
CH_3OOH, pptv	215 ± 149	97 ± 44	196 ± 182	160 ± 103	**514 ± 437**
H_2O_2, pptv	505 ± 431 (480)	115 ± 106 (218)	158 ± 125 (255)	577 ± 420 (468)	**969 ± 675** (808)
HCHO, pptv	237 ± 314 (179)	232 ± 411 (78)	253 ± 225 (206)	180 ± 188 (134)	423 ± 373 (105)
OH, pptv	0.29 ± 0.14 (0.62)	0.35 ± 0.10 (0.36)	**0.47 ± 0.17** (0.80)	0.26 ± 0.08 (0.43)	0.18 ± 0.10 (0.21)
HO_2, pptv	9.08 ± 3.56 (12.5)	5.68 ± 1.48 (7.5)	6.81 ± 2.46 (6.7)	9.54 ± 3.00 (10.7)	**13.09 ± 3.98** (10.5)
Ethane (C_2H_6), pptv	715 ± 268 (637)	537 ± 196 (719)	977 ± 510 (628)	882 ± 193 **(844)**	**1296 ± 1034 (832)**
Ethene (C_2H_4), pptv	3 ± 7	2 ± 3	6 ± 7	7 ± 34	**346 ± 780**
Acetylene (C_2H_2), pptv	80 ± 31	77 ± 38	95 ± 36	**159 ± 40**	**345 ± 440**
Propane (C_3H_8), pptv	138 ± 124 (114)	75 ± 50 (101)	**280 ± 269** (116)	149 ± 99 (145)	251 ±253 (89)
Benzene (C_6H_6), pptv	13 ± 7	9 ± 5	14 ± 10	**24 ± 11**	**130 ± 263**
Toluene ($C_6H_5CH_3$), pptv	5 ± 2	NA[e]	**8 ± 3**	5 ± 2	**53 ± 16**
Acetaldehyde (CH_3CHO), pptv	103 ± 68	118 ± 55	105 ± 78	110 ± 50	**306 ± 331**
Acetone (C_3H_6O), ppbv	1.46 ± 0.85 (0.88)	1.04 ± 0.69 (0.60)	1.61 ± 0.75 (0.86)	2.03 ± 0.91 (0.83)	2.03 ± 0.87 (0.85)
Methanol (CH_3OH), ppbv	1.32 ± 0.75	0.85 ± 0.74	2.01 ± 1.14	**2.21 ± 1.02**	**5.55 ± 2.14**
Ethanol (C_2H_5OH), pptv	96 ± 74	75 ± 71	164 ± 110	156 ± 106	**322 ± 161**
CO_2, ppmv	375.2 ± 2.2	374.3 ± 2.2	374.3 ± 3.3	**373.0 ± 2.2**	373.5 ± 1.9
CH_4, ppbv	1791 ± 16	**1757 ± 34**	1794 ± 20	**1815 ± 13**	**1819 ± 24**
CFC-12, pptv	538 ± 3	**526 ± 9**	538 ± 3	538 ± 3	538 ± 4
CFC-11, pptv	254 ± 2	**243 ± 7**	254 ± 2	254 ± 2	252 ± 2
CFC-113, pptv	78.4 ± 0.6	**75.8 ± 1.7**	78.5 ± 0.8	78.4 ± 0.5	78.5 ± 0.5
H-1211, pptv	4.32 ± 0.11	**4.06 ± 0.21**	4.36 ± 0.10	4.34 ± 0.09	4.31 ± 0.08
^7Be, fCi/m^3	497 ± 675	**2994± 1754**	365 ± 511	764 ± 776	635 ± 548
NO_3^-, pptv	27 ± 52	21 ± 15	25 ± 28	41 ± 40	**501 ± 592**
SO_4^{2-}, pptv	60 ± 42 (50)	**100 ± 36 (72)**	65 ± 48 (40)	**111 ± 55** (81)	**285 ± 261 (87)**
$C_2O_4^{2-}$, pptv	6 ± 5	8 ± 4	6 ± 4	**15 ± 7**	**114 ± 131**
NH_4^+, pptv	70 ± 59 (121)	97 ± 65 (170)	64 ± 49 (101)	**130 ± 61** (230)	**1270 ± 1430 (324)**
Na^+, pptv	105 ± 175	92 ± 105	82 ± 76	130 ± 340	97 ± 99
K^+, pptv	30 ± 44	34 ± 67	25 ± 26	21 ± 20	**166 ± 164**
Mg^{2+}, pptv	7 ± 9	5 ± 6	5 ± 5	11 ± 16	10 ±14
Ca^{2+}, pptv	22 ± 33	15 ± 16	26 ± 35	31 ± 46	21 ± 33
Fine sulfate aerosols, pptv	77 ± 112	73 ± 57	47 ± 44	87 ± 69	165 ± 111
Modeled Asian CO, ppbv	14 ± 7	18 ± 5	14 ± 6	**23 ± 6**	19 ± 2
Modeled NABB CO[d], ppbv	3 ± 2	3 ± 2	2 ± 2	4 ± 3	**28 ± 29**

For each type of airmass we indicate the observed mean ± standard deviation (σ). The mean model results sampled along the flight track are given in parenthesis. Chemical species that are significantly enhanced (> mean + 1σ) or depleted (< mean - 1σ) with respect to background are highlighted in bold.

[a] Nitrogen oxides, NO_x = observed NO_2 + observed NO.

[b] Measurements of total peroxynitrates, $\Sigma PNs \equiv N_2O_5+HNO_4+PAN+PPN+$other organic peroxynitrates.

[c] We define total reactive nitrogen, NO_y, as the sum of observed $NO+NO_2+PAN+HNO_3+HNO_4$.

[d] Modeled North American Biomass Burning (NABB) CO.

[e] NA: Not Available.

Table 3. Observed chemical composition of Asian plumes: Comparison between INTEX-A and other campaigns.

	INTEX-A	**PEM-West B** [a]	**TRACE-P** [a]	**ITCT2K2**	**PHOBEA**
Reference	This work	*Hoell et al.* [1997]	*Jacob et al.* [2003]	*Nowak et al.* [2004] [b] *Brock et al.* [2004] [c]	*Kotchenruther et al.* [2001] [d] *Price et al.* [2004] [e]
Location	North America	NW Pacific (25-50°N; 120 - 150°E)	NW Pacific (25-50°N; 120 - 150°E)	NE Pacific (30-45°N; 115 - 130°W)	NE Pacific (47-49°N; 122 - 126°W)
Altitude	6-12 km	5-10 km	5-10 km	2-8 km	0-8 km
Time Period	July–August 2004	February-March 1994	February-April 2001	April –May 2002	Spring 1997-2002
O_3, ppbv	99 ± 20	56 ± 30	60 ± 25	73 ± 10 [b]	44 – 79 [e]
CO, ppbv	128 ± 14	134 ± 40	138 ± 54	198 ± 40 [b]	153 – 233 [e]
NO_x, pptv	289 ± 201	48 ± 50	90 ± 100	50 ± 40 [b]	19 – 25 [d]
PAN, pptv	592 ± 159	210 ± 153	273 ± 182	360 ± 130 [b]	212 – 308 [d]
HNO_3, pptv	363 ± 304	159 ± 73	234 ± 294	70 ± 10 [b]	
NO_y, pptv [f]	1330 ± 458	528 ± 273	597 ± 353	640 ± 160 [b]	
Ethane, pptv	882 ± 193	1353 ± 430	1243 ± 503	1600 ± 300 [b]	1582 - 1979 [d]
Acetylene, pptv	159 ± 40	396 ± 237	359 ± 254		360 - 504 [d]
Acetone, ppbv	2.03 ± 0.91	0.57 ± 0.16	1.16 ± 0.43	1.4 ± 0.3 [b]	
Methanol, ppbv	2.21 ± 1.02	0.72 ± 0.45	1.80 ± 0.87	1.5 ± 0.5 [b]	
Benzene, pptv	24 ± 11	54 ± 46	69 ± 64	100 ± 100 [b]	66 – 186 [d]
Propane, pptv	149 ± 99	319 ± 177	264 ± 182	300 ± 200 [b]	324-535 [d]
HCN, pptv	420 ± 60		270 ± 78		
CH_3CN, pptv	159 ± 30		159 ± 47	310 ± 100 [b]	
CH_4, ppbv	1815 ± 13	1761 ± 24	1813 ± 21		1827 -1838 [d]
NO_3^-, pptv	41 ± 40	40 ± 28	55 ± 66	34 [c]	
SO_4^{2-}, pptv	111 ± 55	97 ± 58	222 ± 166	94 [c]	
$C_2O_4^{2-}$, pptv	15 ± 7	10 ± 5	17 ± 9		
NH_4^+, pptv	130 ± 61	155 ± 94	193 ± 141		
Na^+, pptv	105 ± 175	196 ± 115	233 ± 147	45 [c]	
K^+, pptv	21 ± 20	45 ± 15	22 ± 20	75 [c]	
Mg^{2+}, pptv	11 ± 16	27 ± 22	44 ± 66	20 [c]	
Ca^{2+}, pptv	31 ± 46	51 ± 39	176 ± 262	73 [c]	

[a] For PEM-West B and TRACE-P, the value listed are the mean ± 1σ of all observations between 5-10 km at [25-50°N, 120-150°E].
[b] Mean ± 1σ of 7 transpacific transport plumes obtained during ITCT2K2 from *Nowak et al.* [2004].
[c] The highest 10% concentration levels obtained during ITCT2K2 from *Brock et al.* [2004].
[d] Mean concentration ranges of Asian airmasses originating north of 40°N or west of 180°W sampled between 2-8 km during the PHOBEA 1999 aircraft experiment [*Kotchenruther et al.*, 2001].
[e] Mean concentration ranges in 6 Asian transpacific transport plumes observed in the free troposphere during the PHOBEA project between 1999 and 2002 [*Price et al.*, 2004].
[f] For PEM-West B and ITCT2K2, NO_y was measured in situ, while for TRACE-P NO_y represents the sum of observed NO_x, HNO_3, and PAN.

Table 4. Transport statistics and chemical characteristics of individual Asian plumes.

	Background	July 1		August 2	July 20	August 14	July 15
		Plume A	Plume B				
Minutes sampled		29	33	102	60	17	14
Export mechanism[a]		Convection	WCB	Convection, Typhoon	WCB	WCB, Typhoon	WCB
Mean theta (K) [b]		328	327	332	328	333	329
Altitude (km) [b]		6.5-11.5	6.5-11.0	7.5-10.5	5-8	8-10	7-10
Transport time [c] (days)		3	5	5-9	8	8-9	9
O_3, ppbv	73	88 (81)	**106** (81)	**110** (**89**)	**93** (77)	83 (80)	73 (66)
CO, ppbv	95	**131** (**125**)	**124** (**111**)	**135** (95)	**125** (**111**)	107 (91)	**117** (**117**)
H_2O, ppmv	719	371	498	455	596	133	869
Relative humidity, %	49	57	60	55	37	52	69
NO_x, pptv	285	136 (48)	161 (42)	266 (166)	411 (193)	415 (100)	392 (84)
PAN, pptv	301	**554** (259)	**484** (295)	**617** (257)	**675** (306)	410 (197)	**567** (341)
PNs, pptv	295	427	373	**547**	**532**	210	**614**
HNO_3, pptv	245	115 (181)	188 (206)	**591** (358)	288 (256)	154 (267)	206 (244)
HNO_4, pptv	53	67	64	**118**	62	39	**98**
NO_y, pptv	884	872 (595)	897 (518)	**1592** (772)	**1436** (749)	1018 (562)	1263 (648)
SO_2, pptv	33	12 (9)	61 (10)	27 (10)	49 (19)	68 (**100**)	38 (9)
HCN, pptv	285	**441**	**447**	**429**	**381**	**472**	**354**
CH_3CN, ppptv	147	158	167	156	155	161	178
CH_3OOH, pptv	215	240	168	130	181	140	134
H_2O_2, pptv	505	**1027** (828)	**1094** (882)	385 (361)	508 (525)	312 (315)	416 (829)
HCHO, pptv	237	NA (70)	NA (70)	133 (134)	199 (216)	315 (50)	281 (223)
Ethane, pptv	715	921 (**1063**)	835 (**1081**)	901 (723)	853 (**814**)	813 (656)	977 (**913**)
Ethene, pptv	3	5	5	4	6	**34**	8
Acetylene, pptv	80	**169**	**156**	**171**	**159**	**130**	**116**
Propane, pptv	138	123 (**218**)	114 (**224**)	147 (104)	156 (134)	194 (91)	226 (164)
Benzene, pptv	13	**30**	**29**	18	**27**	18	**23**
Acetone, ppbv	1.46	**2.59** (0.80)	1.47 (0.86)	2.05 (0.73)	2.29 (0.95)	1.49 (0.54)	1.47 (1.30)
Methanol, ppbv	1.32	**2.60**	1.49	**2.06**	**2.22**	1.90	**3.98**
Ethanol, pptv	96	**234**	58	**169**	86	**213**	**273**
CH_4, ppbv	1791	**1816**	**1808**	**1821**	**1810**	1805	NA
^7Be, fCi/m^3	497	*272*	229	634	**1262**	574	755
NO_3^-, pptv	27	***142***	**103**	35	18	38	19
SO_4^{2-}, pptv	60	***121(137)***	**164 (130)**	90 (49)	**131** (62)	**102 (106)**	56 (94)
$C_2O_4^{2-}$, pptv	6	***12***	**15**	**19**	**14**	8	6
NH_4^+, pptv	70	***172(376)***	**213 (356)**	108 (190)	**136** (157)	107 (186)	70 (190)
Na^+, pptv	105	***1883***	122	44	58	53	166
K^+, pptv	30	*14*	47	14	14	14	59
Mg^{2+}, pptv	7	*13*	10	14	8	**18**	4
Ca^{2+}, pptv	22	***122***	17	22	19	**95**	15
Fine sulfate aerosol, pptv	78	**112**	**160**	38	125	80	67
Model Asian O_3, ppbv	6	**14**	**17**	6	8	9	3
Model Asian CO, ppbv	14	**28**	**34**	**21**	**21**	20	19

Modeled trace gas mixing ratios are shown in parenthesis. For individual Asian plumes, concentrations of trace gases that are significantly enhanced with respect to background are in bold. Numbers in italics indicate that fewer than 5 measurement points were available.

[a] Export mechanisms are determined by examining surface weather charts, SLP fields, and model convective diagnostics.

[b] Altitude range of the plumes sampled by the DC-8 aircraft.

[c] Transport time is estimated using back trajectories.

[e] NA: Not Available.

Figure 1. Structure of the 3 leading Empirical Orthogonal Functions (EOF) identified by Principal Component Analysis applied to observations between 6 -12 km.

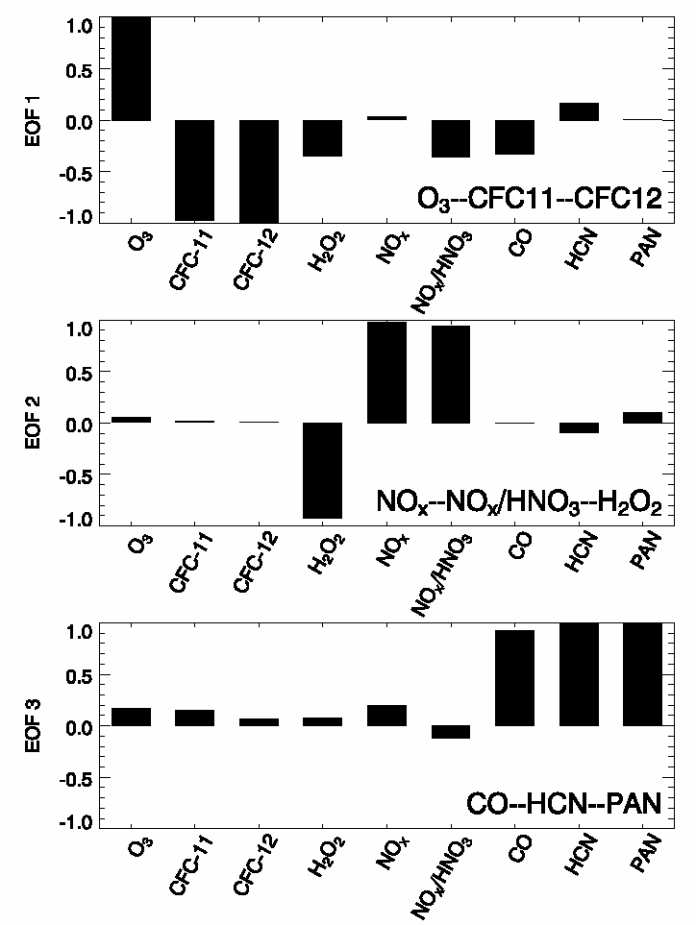

Figure 2. Scatter diagram of observed (a) 10-sec CO and O_3, (b) 75-sec CO and PAN, and (c) 6.5-sec CO and HNO_3, (d) 2-min CO and SO_4^{2-}, (e) 10-sec CO and HCN, (f) 1-min CO and acetylene, (g) 1-min O_3 and NO_y (NO_y = NO + NO_2 + PAN + HNO_3 + HNO_4), (h) 1-min CO and NO_y within different airmasses between 6-12 km during INTEX-A. Biomass burning plumes that have CO > 200 ppbv are not shown here.

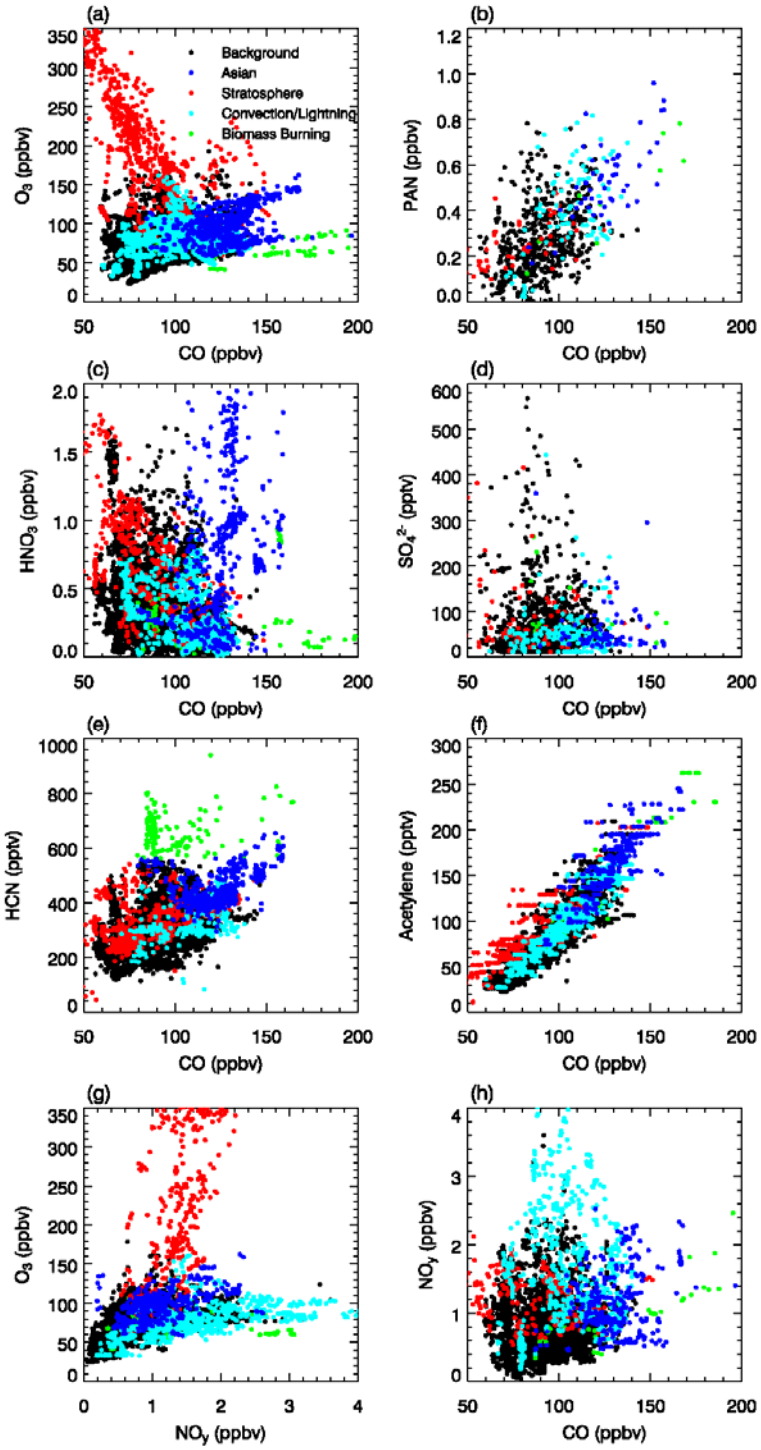

Figure 3. Flight tracks of the NASA DC-8 aircraft during INTEX-A (July 1 – August 14, 2004). Filled circles indicate locations of Asian plumes identified using (a) Principal Component Analysis, (b) the GEOS-Chem Asian CO tracer, and (c) FSU back trajectories, size-scaled and color-scaled according to the observed CO levels.

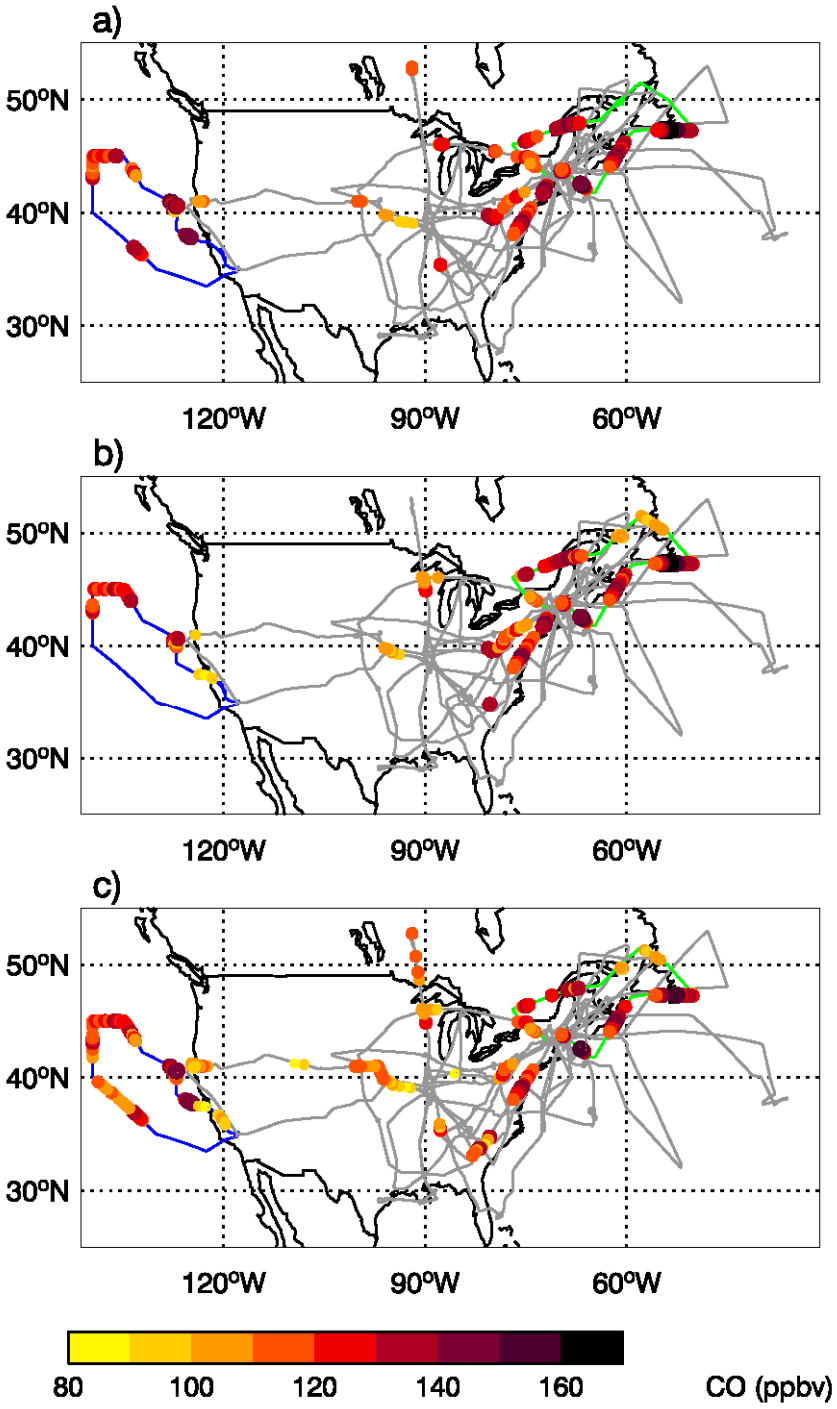

Figure 4. GEOS-Chem Asian CO tracer for the INTEX-A flight on 1 July, 2004. Panel a): Asian CO at 369 hPa (8.8 km) with the DC-8 flight track marked by the write thick line. Locations where plume A and B were sampled were highlighted in red and blue, respectively. Panel b): Curtain plot of Asian CO along the flight track. The black circles with letter "A" and "B" indicate plumes A and B, respectively.

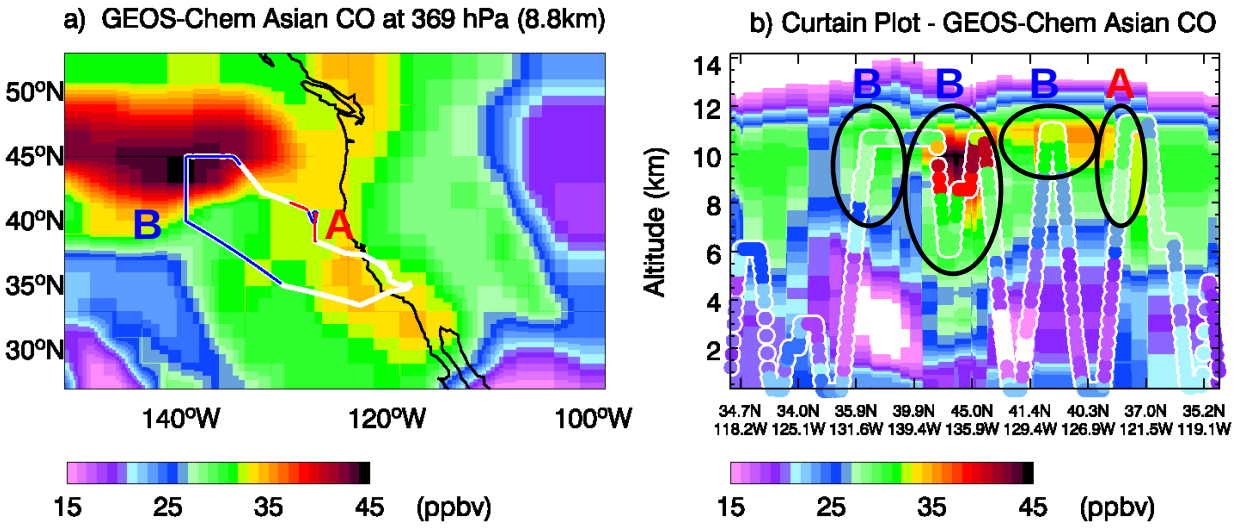

Figure 5. Kinematic back trajectories for the 1 July 2004 Asian plume: 3 day back trajectories for plume A are shown in red and 5 day back-trajectories for plume B are shown in blue. The thick black line indicates the flight track.

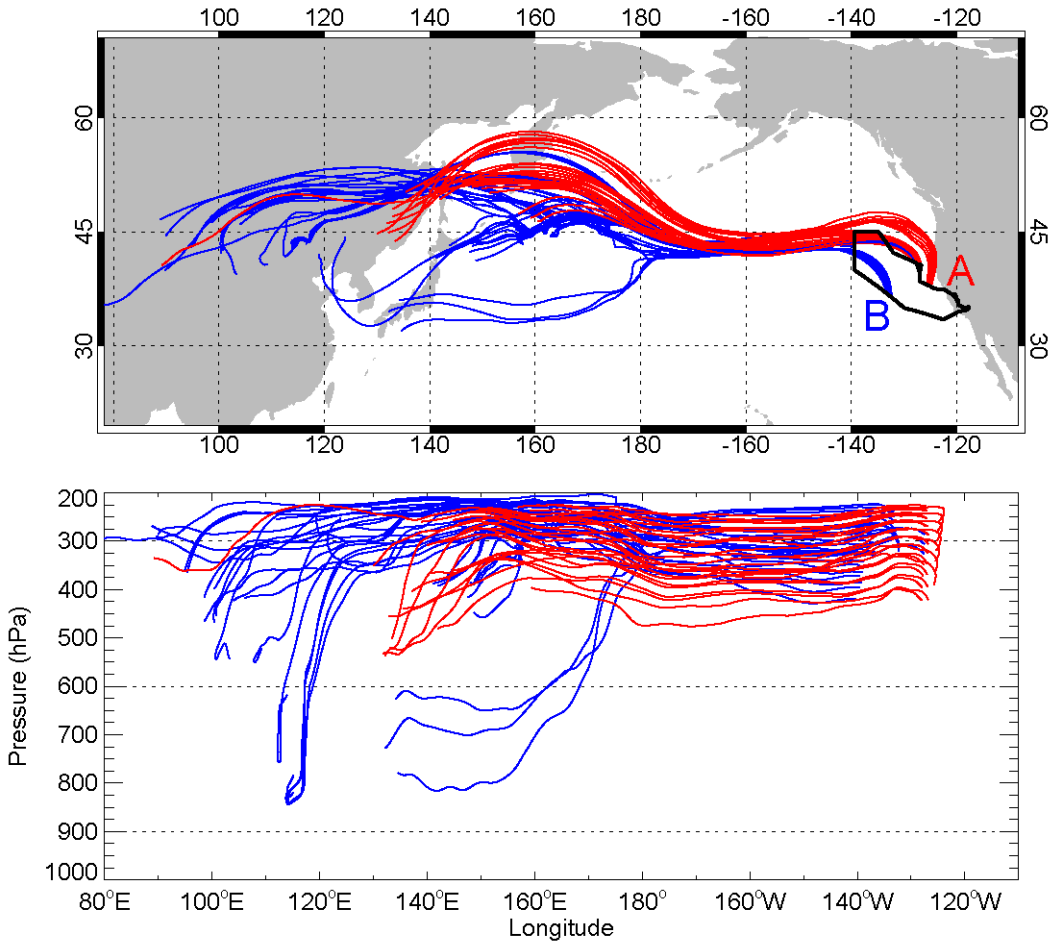

Figure 6. Curtain plots of (a) observed in situ O_3, (b) DIAL O_3, and (c) model O_3 along the 1 July 2004 flight track. The black circles with letter "A" and "B" indicate plumes A and B, respectively.

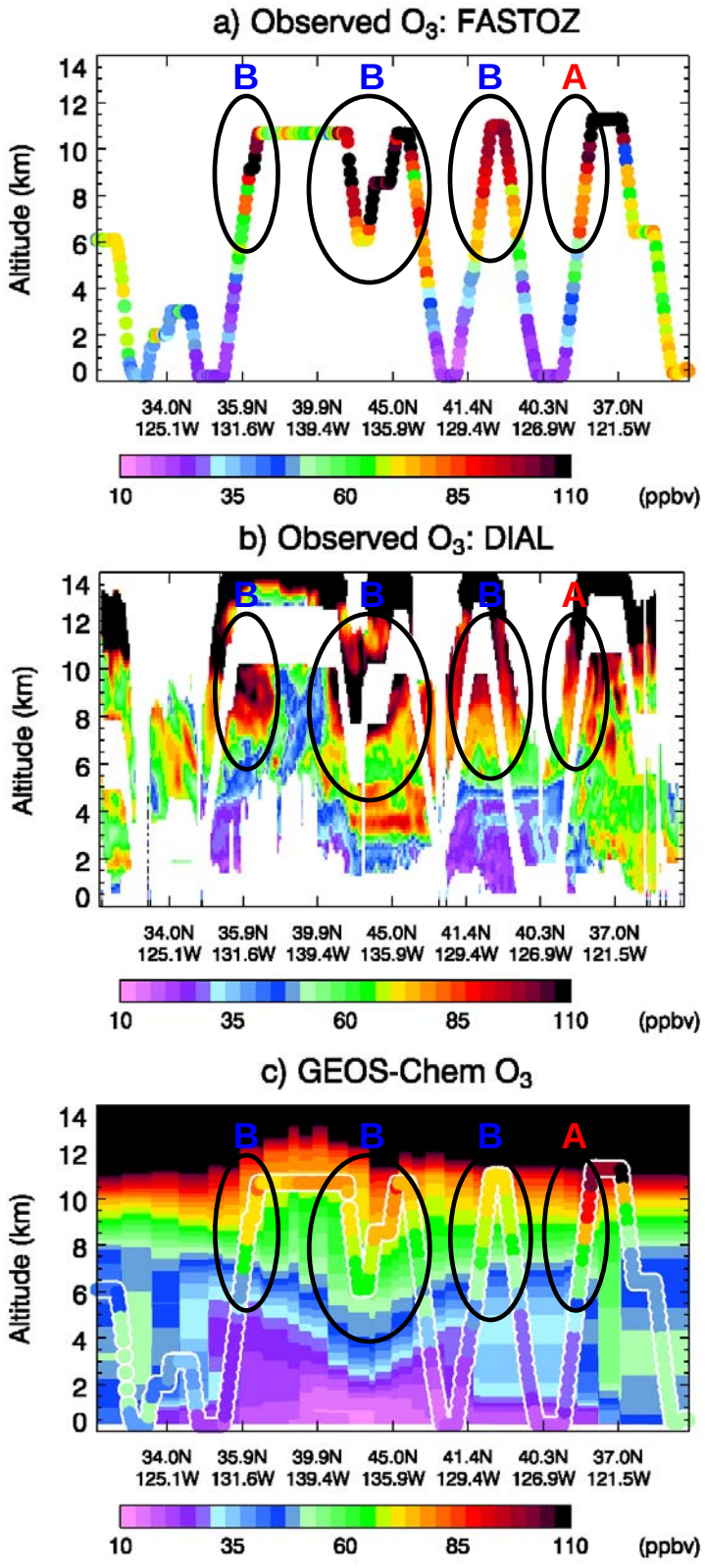

Figure 7. Vertical profiles of observed CO, O_3, HCN, PAN, and fine sulfate aerosols during the 1 July 2004 flight are shown in panels a-b and d-f. Thick gray lines are the mean observed vertical profiles in background air. Scatter plot of CO versus O_3 is in panel c. The two Asian sub-plumes are highlighted in color: plume A in red and plume B in blue.

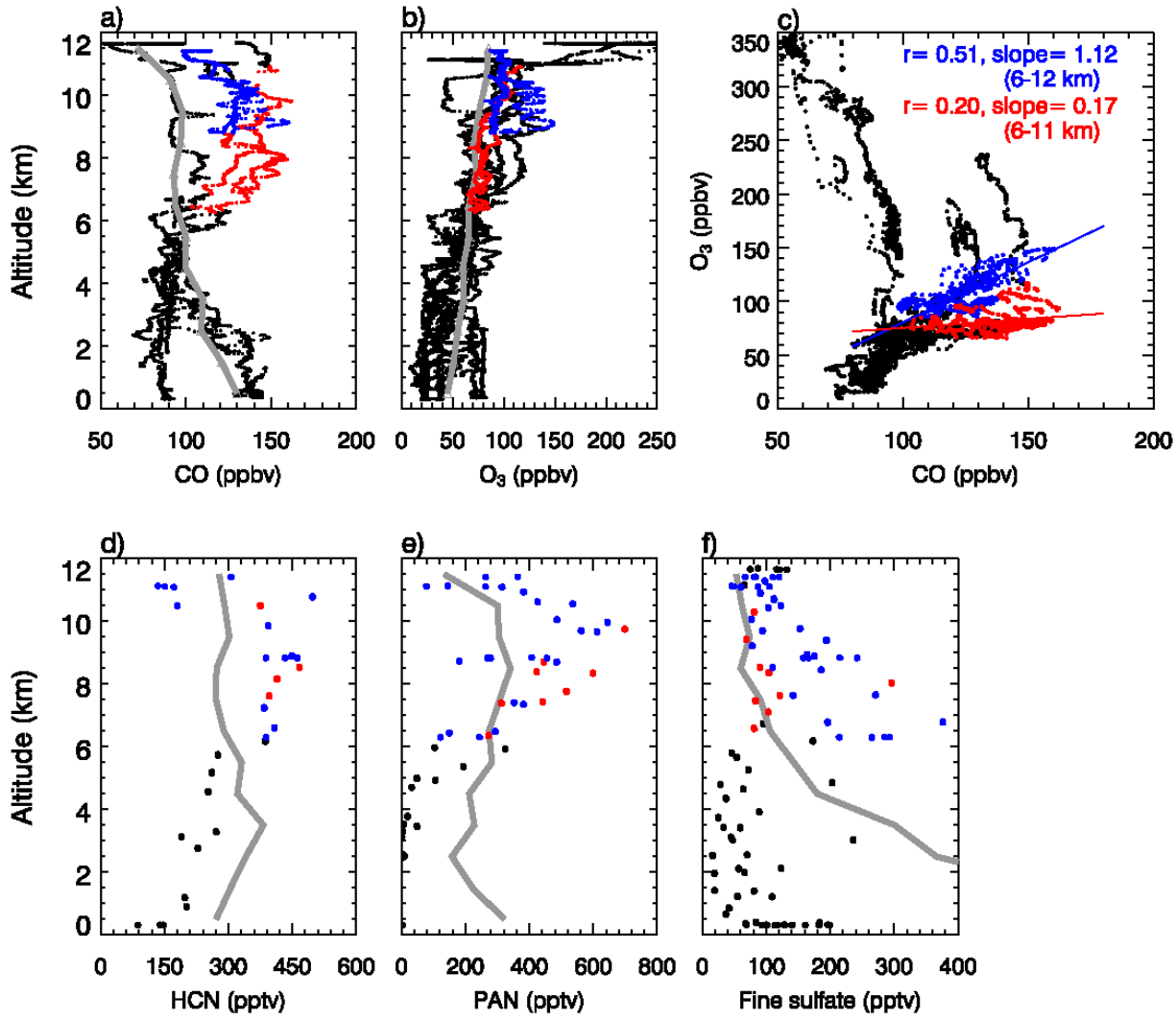

Figure 8. MOPITT CO at 350 hPa (left panels), GEOS-Chem CO (with MOPITT kernel applied) at 350 hPa (middle panels), and GEOS-Chem Asian CO (right panels) at 369 hPa for 26 July, 28 July, 31 July, and 2 August 2004. MOPITT CO is regridded to the model resolution for comparison. Sea level pressure (contours) are also overplotted on the model CO. The white thick line on panel (j) indicates the flight track. The circles and letter "C" and "D" indicates the location of subplumes C and D, respectively.

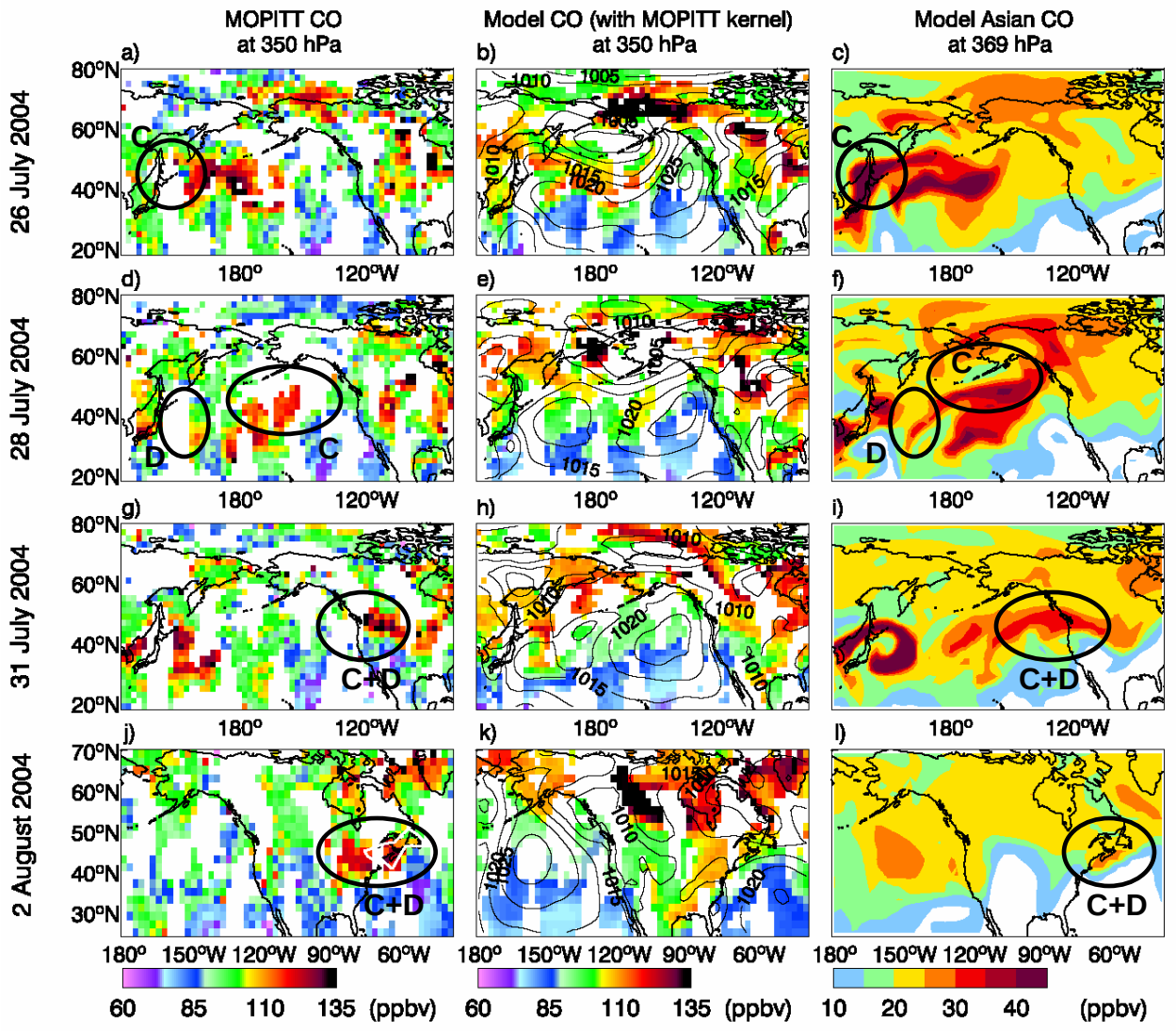

Figure 9. 8 day back trajectories for the 2 August Asian plume. The thick black line indicates the flight track.

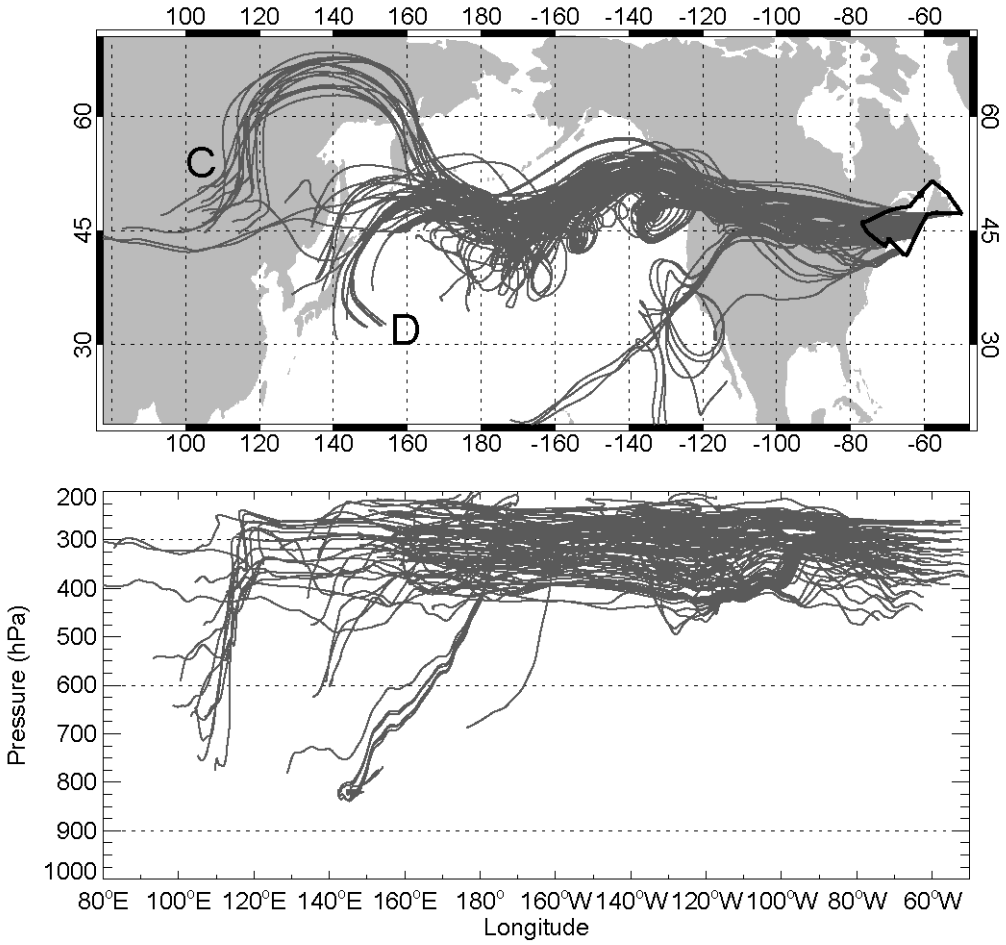

Figure 10. Observed vertical profile of CO, O_3, HCN, and HNO_3 between 14 – 16.4 UTC during the 2 August 2004 flight are shown in panels a and c - e. Note the change in the scale of x-axis in panel c from 0-150 ppbv to 150-400 ppbv. Thick gray lines are the mean observed vertical profiles in background air. Scatter plot of CO versus O_3 is in panel b. The Asian plume is highlighted in blue.